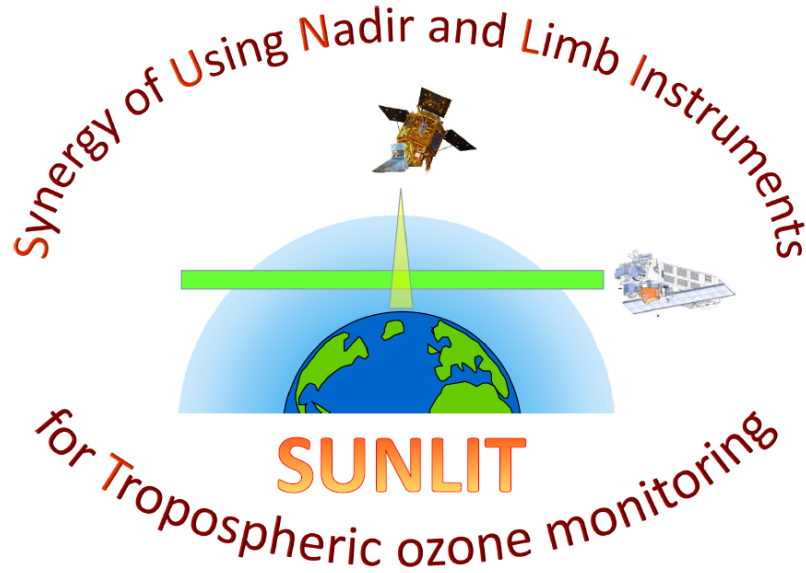




FINNISH METEOROLOGICAL INSTITUTE

ESA SUNLIT – Synergy of Using Nadir and Limb Instruments for Tropospheric  
Ozone Monitoring - ESA AO/1-9101/17/I-NB



## Technical Note

Version: 1.0 (10.12.2020)

Distribution: C. Retscher (ESA) and the FMI SUNLIT team

Prepared by: the SUNLIT FMI team (V. Sofieva, R. Hänninen, M. Szlag, M. Sofiev, J. Tamminen, H.S. Lee)

Reference: SUNLIT-TN-v1

## Contents

1	Introduction .....	3
2	Data and the chemistry-transport model .....	4
2.1	Total ozone column from nadir satellite instruments .....	4
2.2	Ozone profiles from limb satellite measurements .....	5
2.3	SILAM chemistry-transport model .....	6
3	Feasibility studies on residual method to retrieve tropospheric ozone.....	7
3.1	What is observable by the residual method? .....	7
3.2	The effect of vertical integration .....	8
3.3	The effect of sampling and averaging kernel .....	9
3.4	Conclusions from feasibility studies on the residual method.....	10
4	Tropospheric ozone column by the residual method.....	11
4.1	Methodology in general .....	11
4.2	Gridded datasets from nadir instruments .....	11
4.3	Homogenized and interpolated dataset of ozone profiles .....	12
4.3.1	Homogenization of ozone profile data from the limb instruments .....	12
4.3.2	Interpolation of the limb profiles .....	14
4.3.3	Extension in the troposphere .....	15
4.4	Stratospheric ozone column dataset .....	16
4.5	Tropospheric ozone column.....	16
5	A limited validation and examples of data .....	18
5.1	Comparisons of with ozone sondes .....	18
5.2	Comparison with OMI-MLS .....	22
5.3	Comparison with CCD ozone .....	22
6	Summary .....	23
7	Supplementary material .....	24
7.1	Feasibility studies on residual method to retrieve tropospheric ozone.....	24
7.2	Adjusted SILAM ozone field .....	26
7.3	Analyses of small-scale ozone variability using OMI and SILAM data .....	28
7.4	Uncertainties of the interpolated ozone profiles .....	31
7.5	Compatibility of ozone data from limb and nadir instruments. ....	32
8	References .....	32

## 1 Introduction

The satellite measurements in nadir and limb viewing geometry provide a complementary view of the atmosphere. These two measurement systems have their own advantages and limitations. The nadir-looking instruments have a good horizontal resolution; they are good in retrievals of total columns, while the vertical resolution is limited. The measurements in the limb-viewing geometry have usually a good vertical resolution but their horizontal resolution is limited by the spatial sampling and cannot be better than the effective horizontal length of interaction with the atmosphere (a few hundreds of kilometers). The limb profilers allow for a good quality of trace gas retrievals in the stratosphere, while the retrievals from limb instruments in the troposphere are often problematic due to low signal-to-noise ratio and presence of clouds. An effective combination of the limb and nadir measurements of atmospheric composition can provide a new information about atmospheric composition. Successful examples of such combination are tropospheric ozone datasets obtained by subtracting stratospheric columns from the total ozone columns, for OMI nadir and MLS profile measurements (Ziemke et al., 2006), and for SCIAMACHY limb-nadir matching measurements (Ebojie et al., 2016).

The detailed information about the tropospheric ozone is of high importance, because it is nowadays one of the major environmental concerns. Upper tropospheric ozone is an important greenhouse gas, which contributes to global warming. Tropospheric ozone is also a pollutant affecting air quality. It is responsible for respiratory diseases in humans, leads to premature mortality, and causes damage to crops and ecosystems (e.g. Jacobson, 2012; Lippmann, 1991)). It was shown that the amount of tropospheric ozone increased globally during the 20th century due to enhanced emissions of anthropogenic precursors (e.g., Marengo et al., 1994; Shindell et al., 2006).

The retrieval of tropospheric ozone from purely nadir-looking instruments is a challenging, strongly ill-posed problem. Therefore several approaches have been developed: 1) using the spectral information in the nadir satellite measurements (nadir profile retrievals, (Kroon et al., 2011; Liu et al., 2010a, 2010b; Mielonen et al., 2015)), 2) the convective cloud differential (CCD) method applied in the tropics (Ziemke et al., 1998), and 3) via subtraction of stratospheric column from an external source from the total ozone column (the residual method). The retrieval of tropospheric ozone from limb and nadir satellite instruments using the residual approach has already a long history. The first study has been performed in the late 1980s by Fishman and Larsen (1987) who subtracted SAGE stratospheric ozone from total ozone columns by TOMS. Aside from calibration issues involving the use of two different satellite measurements, there was also a serious constraint in producing global data with adequate temporal and spatial coverage due to sparse coverage by the SAGE solar occultation measurements. Several other residual-based approaches have been developed over the years, with combination of TOMS and MLS/UARS (Fishman et al., 1990) and OMI and MLS (Schoeberl et al., 2007; Ziemke et al., 2006, 2011).

The main problems associated with the tropospheric ozone retrievals from nadir and limb measurements are (i) necessity of data calibration and (ii) usually insufficient horizontal

coverage of limb profile measurements. In order to get the stratospheric ozone field with high-horizontal resolution, a 2D interpolation (Ziemke et al., 2006) or wind-trajectory scheme (Schoeberl et al., 2007) is used.

The satellite measurements of total ozone by TROPOMI on Sentinel 5P open new possibilities for monitoring of atmospheric pollutants from space because of their unprecedented horizontal resolution.

The main aim of our work is further development of the methods for assessment of tropospheric ozone using synergy of limb and nadir measurements and apply them to measurements by TROPOMI/Sentinel 5P and OMI/Aura. The novelty of the approach is using measurements from several satellite instruments in limb-viewing geometry for the stratospheric ozone column dataset. In addition, we have performed extensive sensitivity studies using the simulations with the chemistry-transport model (CTM) SILAM (System for Integrated modeLLing of Atmospheric coMposition).

This TN presents the description of the methods developed within the project and some illustrative examples of the created datasets. The main part of the TN contains a concise description of the methods and results. It is organized as follows. Section 2 describes the satellite datasets and the CTM SILAM. Section 3 is dedicated to feasibility studies on retrievals of tropospheric ozone by the residual method, which have been performed using simulations with SILAM. Section 4 describes the retrieval method for tropospheric ozone column developed in the SUNLIT project. Examples of data and some validation results are shown in Section 5. Summary (Section 6) concludes the TN. Additional illustrations are provided in the Supplement.

## 2 Data and the chemistry-transport model

### 2.1 Total ozone column from nadir satellite instruments

In our analyses we use total column ozone data from OMI on Aura (<https://aura.gsfc.nasa.gov/omi.html>, Levelt et al., 2018) and TROPOMI on Sentinel 5P (<http://www.tropomi.eu>; <https://sentinel.esa.int/web/sentinel/missions/sentinel-5p>, Veefkind et al., 2012). OMI and TROPOMI are in sun-synchronous orbits and provide the information at about same local time (1:30 p.m. and 1:45 p.m.). OMI operates since 2004, and its data have been used in different applications including evaluation of trends (Levelt et al., 2018). The OMI ground-pixel size is 13x25 km<sup>2</sup>. TROPOMI operates since 2017. It has a very fine spatial resolution with the ground-pixel size 3.5x 7 km<sup>2</sup> before August 2019 and 3.5 x 5.5 km<sup>2</sup> after that date.

In our work, we use the Level 2 OMI and TROPOMI total ozone columns retrieved with the same GODFIT v4.0 processor (Lerot et al., 2014). Total ozone columns are derived using a non-linear minimization procedure of the differences between measured and modelled sun-normalized radiances in the ozone Huggins bands (fitting window: 325-335 nm). The typical

random uncertainties of total column data, as estimated by the retrieval algorithm, are in the range of 0.5 - 5 DU for OMI and 0.5-2 DU for TROPOMI (Lerot et al., 2014; Sofieva et al., 2020).

## 2.2 Ozone profiles from limb satellite measurements

In our work, we use the data from several limb /occultation satellite instruments. Three of them -MIPAS (Michelson Interferometer for Passive Atmospheric Sounding), SCIAMACHY (SCanning Imaging Spectrometer for Atmospheric CHartography) and GOMOS (Global Ozone Monitoring by occultation of Stars) - operated on Envisat in 2002-2012. Three other limb instruments are still operational: OSIRIS (Optical Spectrograph and InfraRed Imaging System) on Odin, MLS (Microwave Limb Sounder) on Aura and OMPS-LP (Ozone Mapping and Profiles Suite - Limb Profiler) on Suomi-NPP.

The information about the ozone profile data is collected in Table 1. All these satellites are in sun-synchronous orbits, so that the measurements are performed in nearly the same local time, which is instrument-specific. MLS and OMPS measurements are performed in close local times close to OMI and TROPOMI measurements, which is advantageous for the proposed application. The abovementioned limb instruments provide ozone profiles with a vertical resolution of 2-4 km and random uncertainties 1-10 % in the stratosphere (see Table 1 for more details). The horizontal resolution associated with the limb-profile measurement technique is 200-400 km along line of sight. The selected limb instruments provide from ~100 to ~3500 profiles per day (Table 1), which are spaced uniformly in longitudinal direction according to satellite orbits (see also Figure 7).

*Table 1. Information about the datasets used in the analyses*

<b>Instrument/ satellite</b>	<b>Processor, data source</b>	<b>Time period</b>	<b>Local time</b>	<b>Estimated precision</b>	<b>Profiles per day</b>
OSIRIS/ Odin	USask v5.10	2011 – present	6 a.m., 6 p.m.	2-10%	~250
GOMOS/ Envisat	ALGOM2s v1.0	2002 – 2011	10 p.m.	0.5–5 %	~110
MIPAS/ Envisat	KIT/IAA V7R_O3_240	2005 – 2012	10 p.m., 10 a.m.	1–4%	~1000
SCIAMACHY/ Envisat	UBr v3.5,	2002- 2012	10 a.m.	1-7%	~1300
OMPS/ Suomi NPP	USask 2D v1.1.0,	2012- present	1:30 p.m.	2-10%	~1600
MLS/Aura	NASA v. 4.2	2004- present	1: 45 a.m and p.m.	1-7 %	~3500

The accuracy and data coverage are lower in the upper troposphere and the lower stratosphere, as illustrated in Figure 1. For limb-viewing satellite measurements, retrievals in the UTLS are challenging due to presence of clouds and lower signal-to-noise ratio. The average estimated random uncertainties are in the range 5-30 % (Figure 1, center). Not all ozone profiles cover fully the UTLS region (Figure 1, right).

For all limb instruments, we use the ozone profiles from the HARMonized dataset of Ozone profiles (HARMOZ) developed in the ESA Ozone\_cci project (Sofieva et al., 2013),

<http://cci.esa.int/ozone/>. HARMOZ consists of the original retrieved ozone profiles from each instrument, which are screened for invalid data by the instrument experts and are presented on a vertical grid (altitude-gridded profiles are used in our paper) and in a common netCDF4 format. The detailed information about the original datasets can be found in (Sofieva et al., 2013).

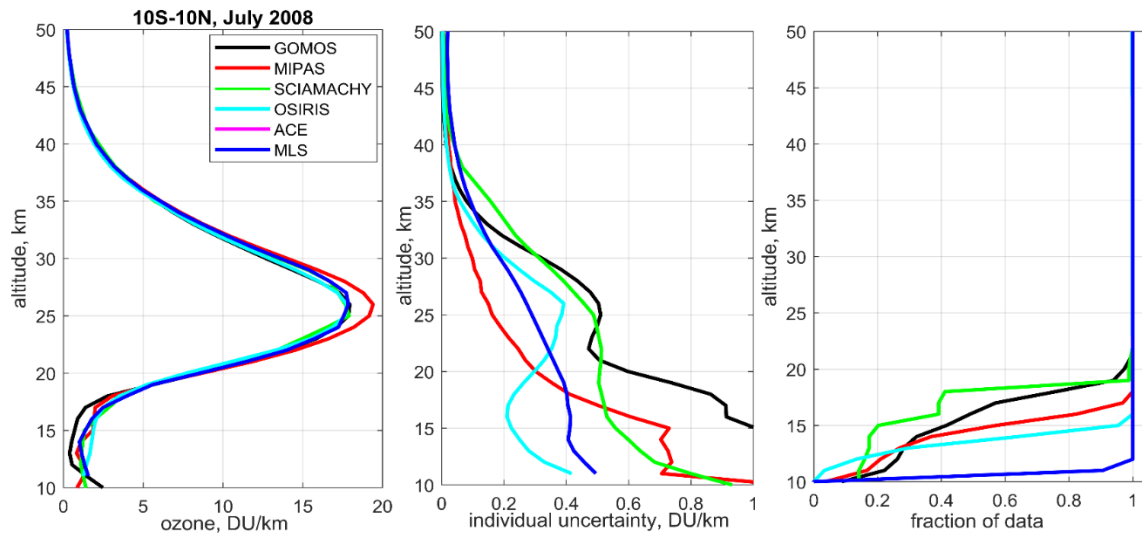


Figure 1. Left: mean ozone profiles at 10S-10N in July 2008. Center: uncertainty of individual ozone profiles, right: fraction of data (with respect to the data in the stratosphere).

### 2.3 SILAM chemistry-transport model

The modelling tool used in the project is the System for Integrated modelling of Atmospheric coMposition SILAM (Sofiev et al., 2015, <http://silam.fmi.fi>). This is an offline chemistry transport model that has several unique features that make it highly suitable for the current project. SILAM is a multi-scale model with seamless scaling from the global coverage down to regional scale with 1-km resolution (Korhonen et al., 2019; Kouznetsov et al., 2020; Sofiev et al., 2018; Xian et al., 2019). SILAM chemical and physical modules cover both the troposphere and the stratosphere (Kouznetsov and Sofiev, 2012; Sofiev, 2002; Sofiev et al., 2020).

SILAM is an extensively evaluated model, a member of the Copernicus Atmospheric Monitoring Service (CAMS) regional European ensemble (<https://www.regional.atmosphere.copernicus.eu/>) and the Panda-MarcoPolo (an EU FP7 project) ensemble for Asia, both operational services with established daily evaluation procedure (Brasseur et al., 2019; Kukkonen et al., 2012; Petersen et al., 2019; Xian et al., 2019). The model has also the extended data assimilation capabilities (Sofiev, 2019; Vira et al., 2017; Vira and Sofiev, 2012, 2015).

In this work, we used the ozone profiles simulated with new development of SILAM v5.7 with the horizontal resolution  $1^{\circ} \times 1^{\circ}$  and the vertical grid as in the ERA-Interim dataset. Compared to v5.6, the new SILAM version has improved photolysis rates, advanced characterization of the clouds and aerosols effects, together with dry and wet deposition where the scavenging has separate parameters for ice and water clouds. For meteorological parameters, we have

moved from ERA-Interim to new ERA5 data set which has 1 hour time resolution. In addition, the newly implemented CBM05 (Carbon Bond Model from year 2005) chemistry module ([http://www.camx.com/files/cb05\\_final\\_report\\_120805.aspx](http://www.camx.com/files/cb05_final_report_120805.aspx)) now provides better tropospheric ozone concentrations, especially in tropics and in remote regions, compared with the previous CBM4 chemistry (Carbon Bond Model version 4, (Gery et al., 1989) and updates). During the SUNLIT project we included also the OTAG (Ozone Transport Assessment Group) update, which improves the oxidant formation at low NO<sub>x</sub> conditions (Yarwood and Burton, 1993) together with updated isoprene chemistry(Whitten et al., 1996) (Whitten et al., 1996).

For anthropogenic emissions, we use CAMS global emission database (v2.1) together with EDGAR4.3.2 emissions for aviation and partly self-made emissions for most important CFC-compounds. In addition, SILAM takes into account biogenic emissions for isoprene and monoterpene (database based on the MEGAN model), sea-salt emissions (including its small bromine fraction), dust-emissions, and NO<sub>x</sub> emissions from lightnings. Emissions from fires are also included, either using IS4FIRES (see: <http://silam.fmi.fi/fires.html>) or different emission inventories.

In majority of analyses presented in our paper, daily averaged ozone fields are used.

### 3 Feasibility studies on residual method to retrieve tropospheric ozone

#### 3.1 What is observable by the residual method?

About 90% of ozone is in the stratosphere (the ozone layer). Figure 2 shows a typical ozone profile for the equatorial region, in units of DU/km, with indicated contributions from different layers. The challenges associated with the residual method are clearly seen in Figure 2: the ozone in the UTLS has nearly the same abundance as the lower tropospheric ozone.

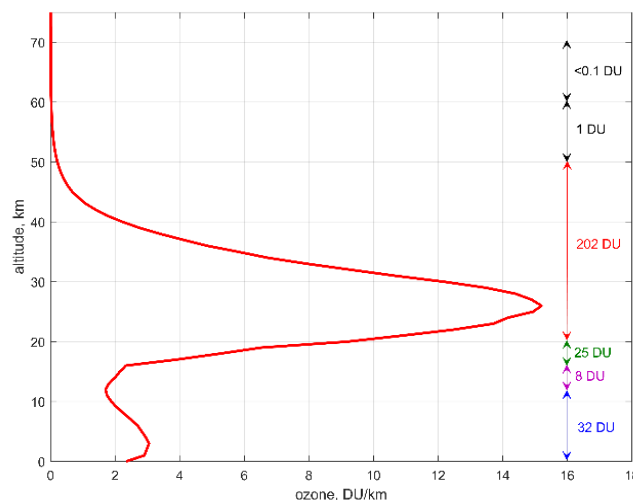


Figure 2 Typical ozone profile for the equatorial region, with indicated contributions of different layers to the total ozone column.

To facilitate the development of the residual method and find the best feasible spatio-temporal resolution for the dataset, we have performed various feasibility analyses with the SILAM CTM. In our analyses, we used the full model data and those sub-sampled at locations and time of satellite measurements.

Throughout this TN, the thermal tropopause definition is used (WMO, 1957). In some special cases at high latitudes, when this definition fails to find the tropopause, we use the ozonepause as a boundary separating the troposphere and the stratosphere. We define the ozonepause as the altitude where the ozone concentration drops (looking from the stratosphere) down to 3.5 DU/km.

### 3.2 The effect of vertical integration

The residual method provides the integrated tropospheric ozone column. When considering the tropospheric ozone column, it is expected that the ground-level ozone enhancements will be smeared out and displaced due to advection. This feature is illustrated in Figure 3, which compares the ground-level SILAM ozone data (Figure 3, left panels) with the tropospheric ozone columns (Figure 3, center and right) for 1 July 2008.

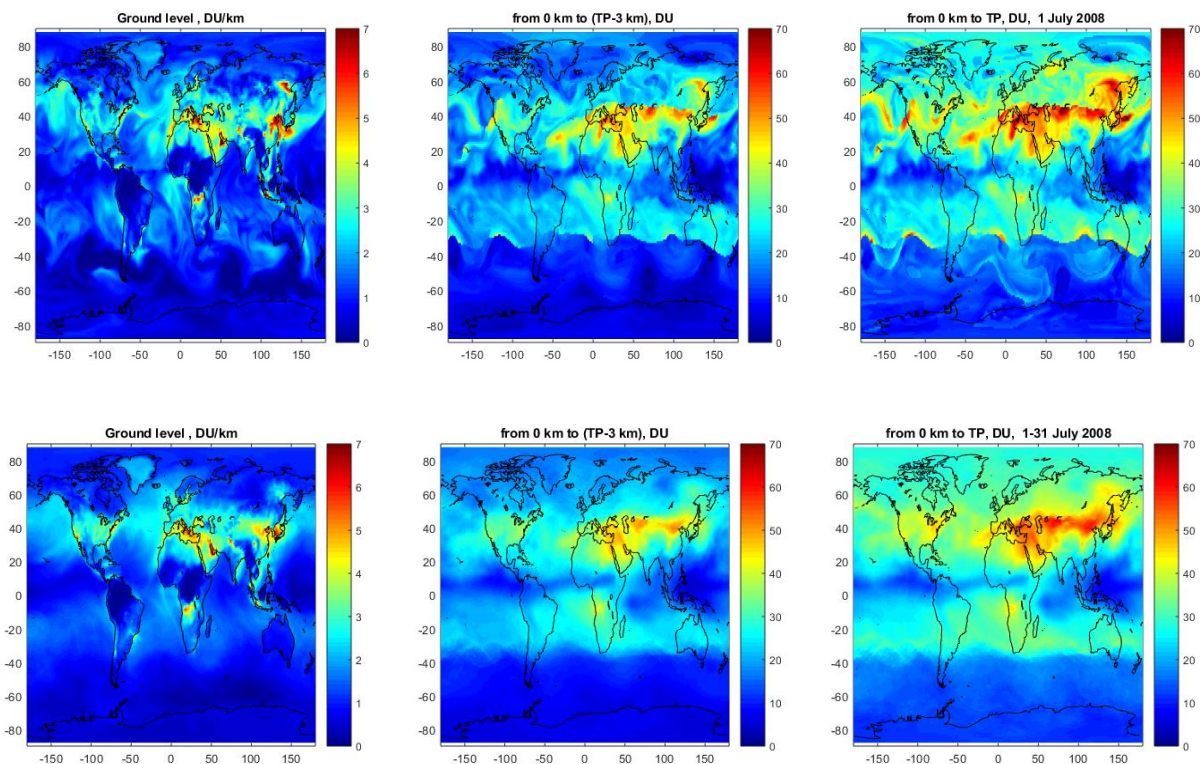


Figure 3. Top panels: simulations with SILAM for 1 July 2008; ground level ozone (left panel) and tropospheric columns: from ground to the altitude 3 km lower than the tropopause (TP-3 km, center panels) and the full tropospheric column up to the tropopause (right panels). Bottom panels show average for July 2008 values.

As seen in Figure 3, tropospheric ozone column (integrated from the surface to the tropopause and referred hereafter to as full tropospheric ozone column, full TrOC, Figure 3 right) has a large portion from the UTLS region, so that the tropospheric features are

significantly blurred in the tropospheric column. If consider the altitude range from the ground to 3 km below the thermal tropopause (referred to as truncated TrOC, Figure 3 center), the influence of the UTLS is smaller but still significant.

In monthly averaged fields (Figure 3, bottom panels), the ground level ozone enhancements are visible, but they are smoothed and sometimes displaced from sources. Some sources (e.g., over Indonesia) are not seen in tropospheric ozone column data. The choice of the upper limit of the tropospheric ozone integration (up to tropopause or below, compared central and right panels in Figure 3) influences the overall level of tropospheric ozone column (as expected) and also the contrast of local enhancements. Therefore, the tropospheric ozone column below the tropopause is advantageous for detecting ground level sources.

Since the quality of limb-profile data (both accuracy and coverage) in the UTLS is limited, one can consider possibility of estimating the upper tropospheric ozone (for example, 3 km below the tropopause) and subtracting it from the full TrOC (analogy of ghost column correction in retrievals from nadir-looking instruments). In real applications, such correction can be done using ozone profile climatology or modelled data. To illustrate the effect, we simulated two approximate corrections of the upper tropospheric ozone. In the first correction, the upper tropospheric (3-km below the tropopause, UT) monthly zonal mean UT ozone column was computed from SILAM data, for each latitude, and subtracted from each data point of full TrOC, for each day. In the second correction, the UT ozone column correction is done using the tropopause-related ozone climatology TpO3 (Sofieva et al., 2014). We found that even such very approximate upper tropospheric ozone corrections give the monthly map of truncated TrOC nearly identical to the true one (Figure S1, right panels), with the difference to the true values mostly smaller than  $\pm 3$  DU.

### 3.3 The effect of sampling and averaging kernel

The coverage by limb instruments is limited. The examples of daily sampling patterns by the limb instruments can be found in Sect. 4.3 of this TN. If the monthly mean stratospheric ozone column (SOC) is computed via simple averaging the data with such sampling, the resulting SOC has significant deviations from the SOC computed using the full ozone field, because different pixels are covered by data from different days. This implies that the monthly average of tropospheric ozone column must be constructed from daily values. The approach of averaging first the stratospheric ozone column and then subtracting it from the averaged total ozone column produce pronounced errors, due to limited sampling by limb instruments (illustration can be found in the Supplement, Figure S2).

Tropospheric column computed via averaging daily TrOC, which is obtained by the residual method, are rather closer to the true distribution using the data with full coverage. This is illustrated in left and central panels of Figure 4. The right panel of Figure 4 shows an analogous estimate of the tropospheric ozone, in which the total ozone column was computed with the OMI averaging kernels taken into account (the examples of OMI and TROPOMI averaging kernels are shown in supplementary Figure S3). Since OMI and TROPOMI

are sensitive to middle and upper tropospheric ozone (Figure S3), the tropospheric ozone column derived by the residual method is of reduced magnitude, compared to the tropospheric ozone column without averaging kernel applied. An interesting feature, which is associated with the influence of averaging kernel, is that the enhancements over central Africa are shifted to Atlantic Ocean. This is a combined effect of OMI low sensitivity near the ground and wind advection of both ozone and its precursors.

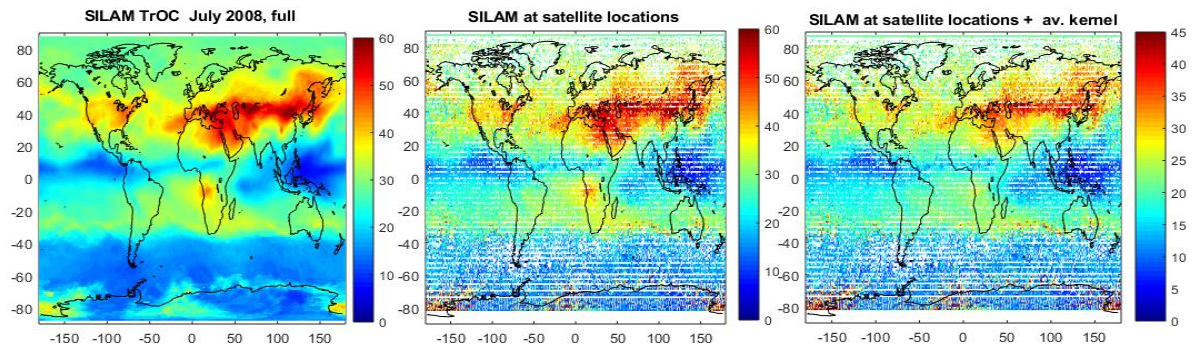


Figure 4. Estimates of full tropospheric ozone column (from the ground to the tropopause) using the application of the residual method to SILAM ozone profiles, monthly average for July 2008. Left: TrOC using the full SILAM ozone field, center: SILAM data sub-sampled at locations of nadir and limb satellite instruments. Right: averaging kernel is taken into account in computing total ozone column at OMI locations.

### 3.4 Conclusions from feasibility studies on the residual method

The following main conclusions can be drawn from the feasibility studies:

- In order to detect ground enhancements of tropospheric ozone, the stratospheric and the UTLS contribution should be accurately removed from the nadir total ozone column data, because the UTLS ozone contribution is comparable with the lower-tropospheric ozone abundances.
- The sensitivity of nadir-looking satellite instruments is limited in the lower troposphere, therefore the observed ground-level ozone enhancements are seen as shifted from the sources and blurred, as a consequence of atmospheric motions and chemical transformations.
- Due to large variability of ozone field and limited sampling by satellite instruments, monthly average tropospheric ozone column from combination of nadir and limb instruments, should be computed from daily tropospheric ozone column.
- Upper tropospheric ozone column correction using the data from an external source is an attractive approach, which allows removal of the UT contribution from the full tropospheric ozone column without introducing large uncertainty into the truncated tropospheric ozone column.

Based on these studies, we have developed the method of estimating the tropospheric ozone column using the combination of limb and nadir measurements. The specific feature of our method is using the CTM-simulated ozone field in creating high-spatial-resolution ozone field,

in the stratosphere and the UTLS. In the next section we present the detailed description of the retrievals.

## 4 Tropospheric ozone column by the residual method

### 4.1 Methodology in general

We follow the general idea of the residual method, which consists of (1) creating clear-sky total ozone column from nadir instruments; (2) creating high-horizontal resolution stratospheric ozone column by combining ozone profiles from several limb instruments, and (3) evaluating the tropospheric ozone column as the difference between total and stratospheric columns.

In our studies, we created first daily tropospheric ozone column data with  $1^\circ \times 1^\circ$  spatial resolution, and then computed monthly averaged data from them.

Below we discuss all steps in detail. The most challenging part in our analysis is creating the merged stratospheric ozone column dataset.

### 4.2 Gridded datasets from nadir instruments

For creating daily gridded total ozone column in  $1^\circ \times 1^\circ$  latitude-longitude bins (which are often referred to as Level 3), we used the clear sky Level 2 data, with cloud fraction less than 0.2.

Since the OMI row anomaly is not fully characterized by the processing flags, an additional data filtering is applied. First, we removed flagged pixels and also one additional row from the left and the right of the flagged region. The presence of row anomaly was also checked by evaluation of ozone difference in adjacent rows. If the values higher than 100 DU are detected, the whole region from two "ozone jumps" is removed. Finally, only the data with relative uncertainty less than 4% are used for creating daily gridded data.

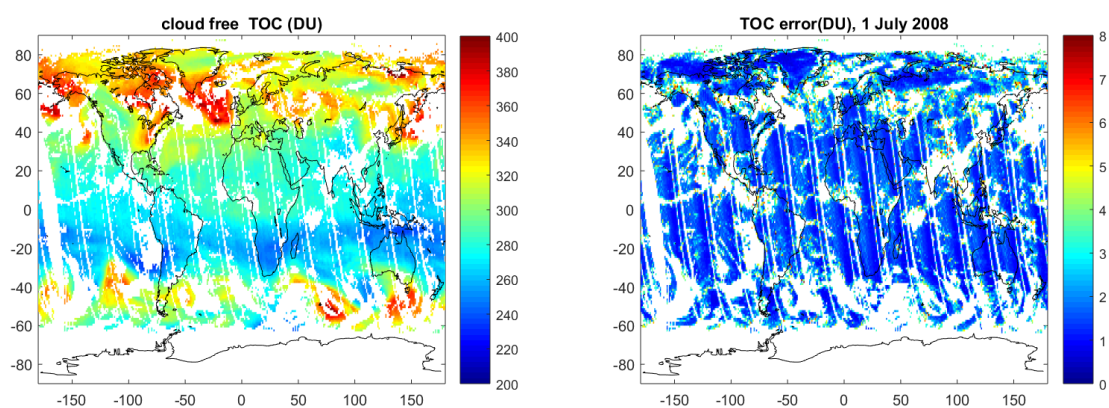


Figure 5. OMI Level 3 total ozone column data (left) and random uncertainty (right) for 1 July 2008

In each latitude-longitude bin, the mean of total ozone column data is evaluated. The uncertainty of the total ozone column is computed as:

$$\sigma^2 = \frac{1}{N} \sum_i \sigma_i^2 + \frac{1}{N} \text{var}(\rho_i) \quad (1)$$

where  $\sigma_i$  are uncertainties and  $\text{var}(\rho_i)$  is the variance of  $N$  individual ozone values in the bin. The typical daily gridded clear-sky total ozone column and the corresponding random uncertainties are shown in Figure 5.

The daily average gridded TROPOMI total ozone column data are computed in a similar way, with the same spatial resolution  $1^\circ \times 1^\circ$ .

### 4.3 Homogenized and interpolated dataset of ozone profiles

In our approach, we first create the  $1^\circ \times 1^\circ$  gridded and interpolated dataset of ozone profiles, and then we compute stratospheric column via integration of ozone profiles. We selected such approach because the limb instruments have limited accuracy and highly non-uniform coverage in the UTLS, while the accurate knowledge of the UTLS profiles is essential for application of the residual method.

In our algorithm, the creation of homogenized interpolated dataset of ozone profiles consists of three main steps:

- (1) Homogenization of ozone profile data from the limb satellites;
- (2) Interpolation of the limb profiles from each day to  $1^\circ \times 1^\circ$  horizontal grid;
- (3) A smooth transition to the adjusted model data below the tropopause.

Below we present the detailed description of the processing.

#### 4.3.1 Homogenization of ozone profile data from the limb instruments

For horizontal interpolation, the data from different satellite measurements should be made compatible. As the first step of such data homogenization, biases between datasets are removed.

We use MLS as a reference dataset. For all other instruments, the biases with respect to MLS are evaluated for each month and for each latitude (with  $1^\circ$  increment), using  $10^\circ$  overlapping zones and corrected via adding latitude-dependent offset. This procedure removes efficiently the biases between limb datasets, as illustrated in Figure 6. After the bias correction, data from different instruments can be used together. An example of bias-corrected data is shown also in Figure 7 (left panel).

The optimal implementation of our horizontal interpolation method (see Sect. 4.3 for details) requires that the error estimates from different instruments agree and realistically describe the variations caused by random data uncertainties. However, this is not the case for the considered limb instruments: while biases between the instruments are rather small (within 10%), the estimated uncertainties can differ by a factor of magnitude. This is illustrated in Figure 7, which show ozone and the reported uncertainties at 10 hPa for MLS, OSIRIS and OMPS-LP (processed by University of Saskatchewan v1.1.0). Uncertainty estimates of OMPS data processed by University of Bremen have smaller difference with respect to MLS,

but they still can differ by the factor 2-3. The difference in error estimates depends on latitude, altitude, and season.

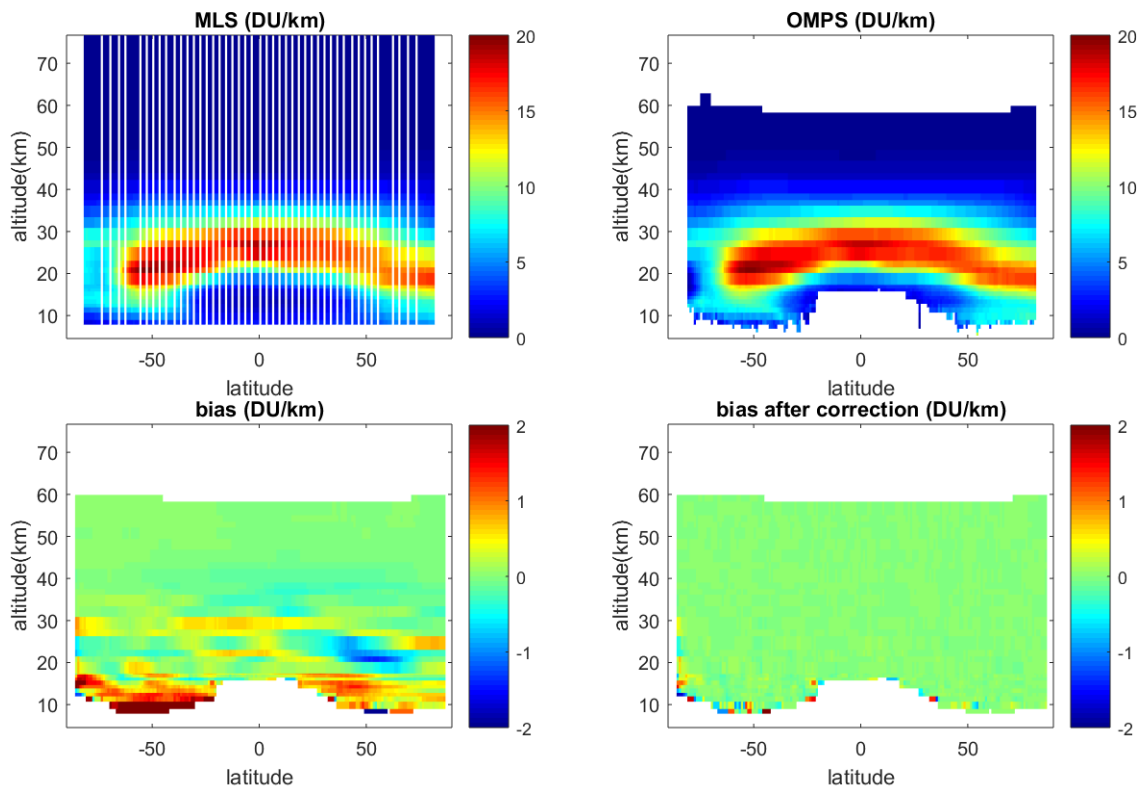


Figure 6. Illustration of the bias correction for September 2018. Upper panel: MLS and OMPS profiles averaged over latitude zones and over the month. Bottom panels: estimated biases before (left) and after(right) bias correction.

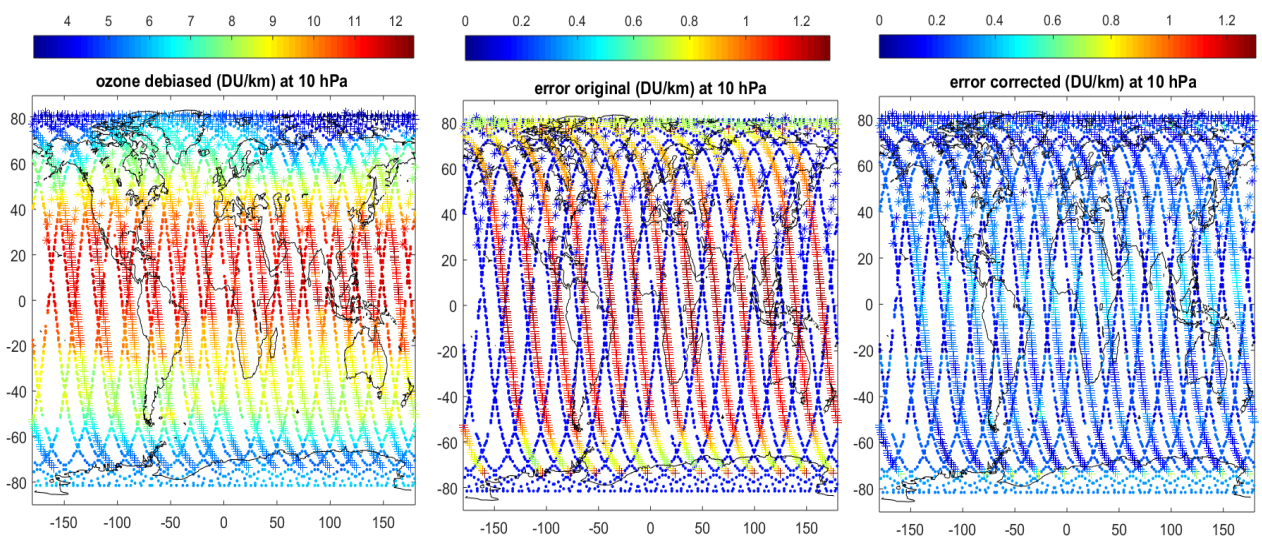


Figure 7. Debiased ozone at 10 hPa for 1 Sep 2018 (left), corresponding original uncertainties (center), and corrected uncertainties (right). MLS data are indicated by dots, OSIRIS - by stars and OMPS by plusses.

Therefore, we applied a simple approach that provides the random uncertainties that are consistent with the variability field. For each instrument and each month, we evaluated sample variance  $s^2$  in  $10^\circ$  latitude zones from experimental data and the SILAM-adjusted field, which is sub-sampled at measurements locations (the creation of SILAM-adjusted ozone dataset is described in Supplement, Sect. S2). The SILAM-subsampled sample variance provides the estimated of the natural variability  $\sigma_{nat}^2$ . Then a posteriori (ex-poste in von Clarmann et al. (2020) terminology) uncertainties can be estimated as  $\sigma_{ex-poste}^2 = s^2 - \sigma_{nat}^2$ . We computed latitude and altitude dependent offset  $\Delta = \sigma_{ex-poste} - \sigma_{ex-ante}$  ( $\sigma_{ex-ante}$  is the mean error estimate provided with profiles, in the same  $10^\circ$  latitude zones over the month) and apply it to each profile. As shown in the right panel of Figure 7, this simple correction of the uncertainty estimates makes them comparable. By the construction, they are compatible with the observed ozone variability.

### 4.3.2 Interpolation of the limb profiles

After homogenization the limb data, they are interpolated to form a high-spatial resolution dataset. For our application, the most attractive approach is a kriging-type interpolation, in which both data uncertainty and the structure of the data variability are taken into account. In this approach, the value at the point  $\mathbf{r}$  is taken as a weighted mean of data in some neighborhood:

$$x(\mathbf{r}) = \sum_i w_i x(\mathbf{r}_i), \quad (2)$$

with the weights  $w_i$  inversely proportional to the total uncertainties:

$$\sigma_{tot,i}^2 = \sigma_{noise,i}^2 + D(\mathbf{r}_i - \mathbf{r}), \quad (3)$$

where  $\sigma_{noise}^2$  is the estimate of the noise in the data, and  $D(\mathbf{r}_i - \mathbf{r})$  is the uncertainty due to the spatial mismatch, which is usually estimated via the structure function (see Supplement S3 for details). In our interpolation method,  $D(\mathbf{r}_i - \mathbf{r})$  is taken from the model-adjusted field, for each day. The weighted mean is assessed using the  $10^\circ \times 20^\circ$  latitude -longitude area around each point.

We have tested our interpolation scheme on noise-free and noisy simulated data with SILAM and found that the kriging-type interpolation described above is superior to the triangulation-type interpolation (for example, natural neighbor interpolation, Sibson et al., 1991): the interpolation error is smaller and fine structures are better resolved. For noisy simulated data, the interpolation error is the smallest if the uncertainty estimates in Eq. (3) are realistic, as expected.

In our method, the interpolation of ozone profiles is performed at each pressure level separately. The example of the interpolated field is shown in Figure 8.

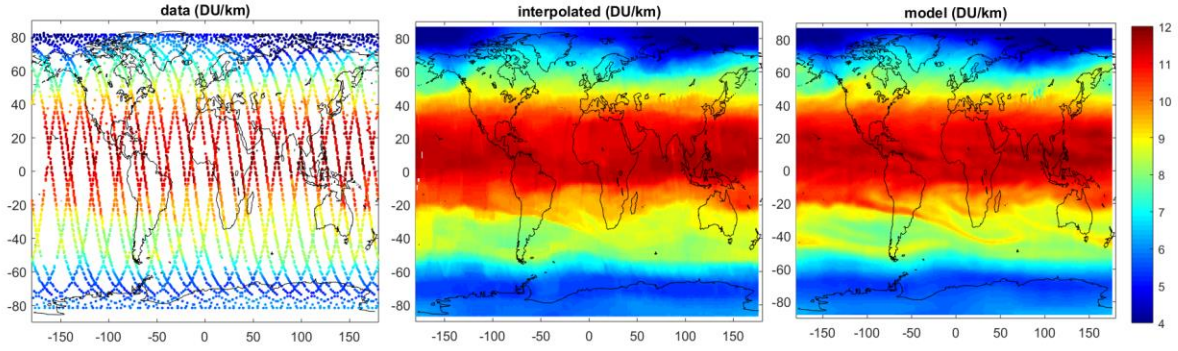


Figure 8 Left: ozone at limb satellite measurements at 10 hPa on 1 September 2018. Center: after interpolation. Right: corresponding adjusted SILAM ozone field at the same pressure level.

The uncertainties of the interpolated field are estimated as follows. The uncertainty after the kriging is estimated as the minimal value of  $\sigma_{tot}$  (Eq.(3)) in the bin used for weighted mean. In addition, we estimated the interpolation uncertainty using the SILAM data: we run the same interpolation on SILAM ozone sub-sampled at measurements location, and evaluated the error as the absolute difference of true and interpolated data. The final uncertainty is the root-mean-square of error propagation and model-assessed interpolation errors. The illustration of uncertainty estimation in the interpolated ozone field is illustrated in Supplement, Sect. S4.

#### 4.3.3 Extension in the troposphere

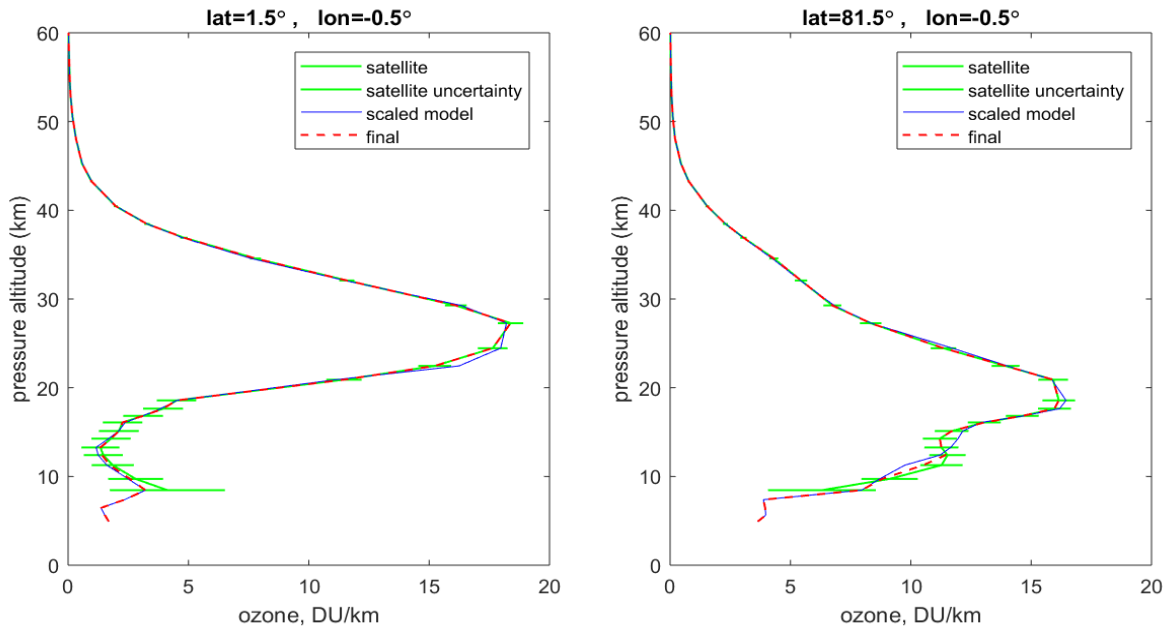


Figure 9. Illustration of transition to model-adjusted profiles at lower altitudes

Since satellite data have limited accuracy, non-homogeneous and rather scarce coverage below the tropopause, we extended satellite-based ozone profiles to lower altitudes

by using the smooth transition to the SILAM-adjusted profiles. The linear transition is performed in such way that above 200 hPa the profile follows fully experimental data and below 400 hPa fully model data. The illustration of the transition to model data at lower altitudes is shown in Figure 9, for tropical and polar atmospheres.

Below in this TN (Sect.5), we show that the resulting ozone profiles are in a good agreement with ozonesonde data.

#### 4.4 Stratospheric ozone column dataset

The computing the stratospheric ozone column from high-resolution profiles is rather straightforward. The integration can be done from the tropopause upwards (we use 55 km as the upper integration limit), or from a certain altitude level. The uncertainties are estimated using the error propagation. The examples of stratospheric ozone columns from the tropopause and from 3 km below the tropopause and corresponding uncertainties are shown in Figure 10.

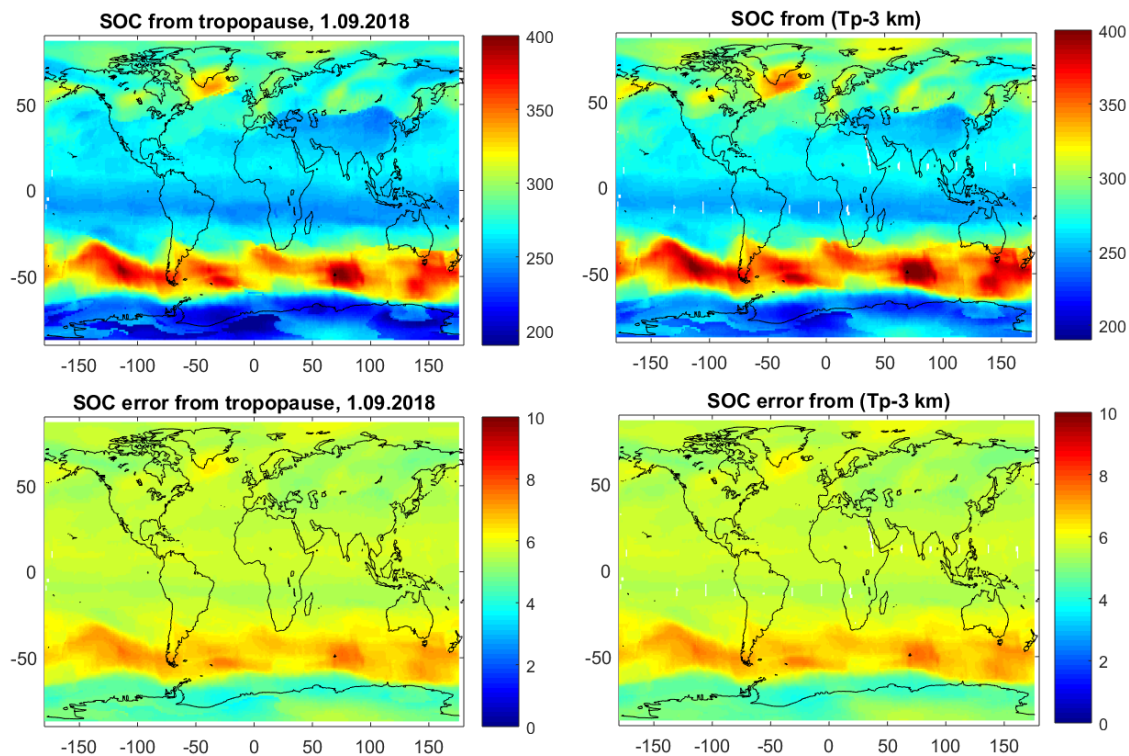


Figure 10. Stratospheric ozone column (DU) from tropopause (left top) and from 3 km below the tropopause (right top). The corresponding uncertainties are shown in bottom panels.

#### 4.5 Tropospheric ozone column

Once the high-resolution stratospheric ozone column dataset is created, the application of the residual method is straightforward: they are subtracted from clear-sky measurements by nadir sensors, daily. The daily values can be averaged to monthly mean values.

However, before the application of the residual method, the compatibility of limb and nadir data should be checked. For this, we compared OMI and TROPOMI measurements in cloudy conditions (the ghost column is removed) with the integrated ozone profiles from the cloud-top height. For this comparison, we selected cloudy pixels with cloud fraction  $>0.8$  and cloud-top pressure less than 350 hPa and the corresponding limb profiles from SILAM adjusted field. We found that over Indonesia and Western Pacific where high clouds are observed, the mean difference between nadir and limb instruments is very small,  $\sim 2$  DU, for both instruments. Therefore, no additional offsetting nadir total columns is performed. The illustrations of this comparison can be found in Supplement S5.

The resulting tropospheric ozone distributions from OMI and TROPOMI for September 2018 are shown in Figure 11. Zooms on China and USA are shown in Figure 12.

Illustrations of the tropospheric ozone are presented also in Sect. 5.

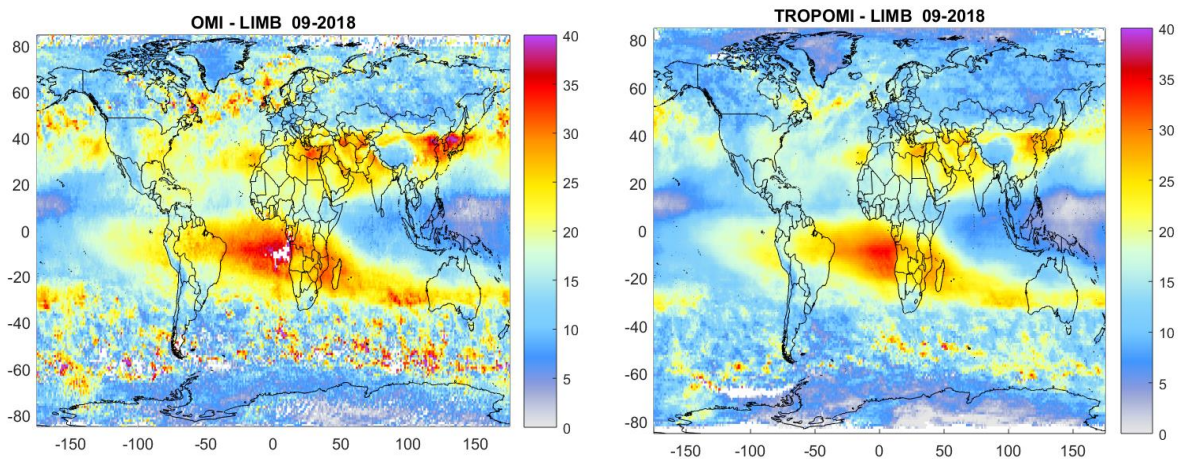


Figure 11. SUNLIT tropospheric ozone distributions for September 2018, from OMI (left) and TROPOMI (right). The stratospheric ozone column is estimated from 3 km below the tropopause.

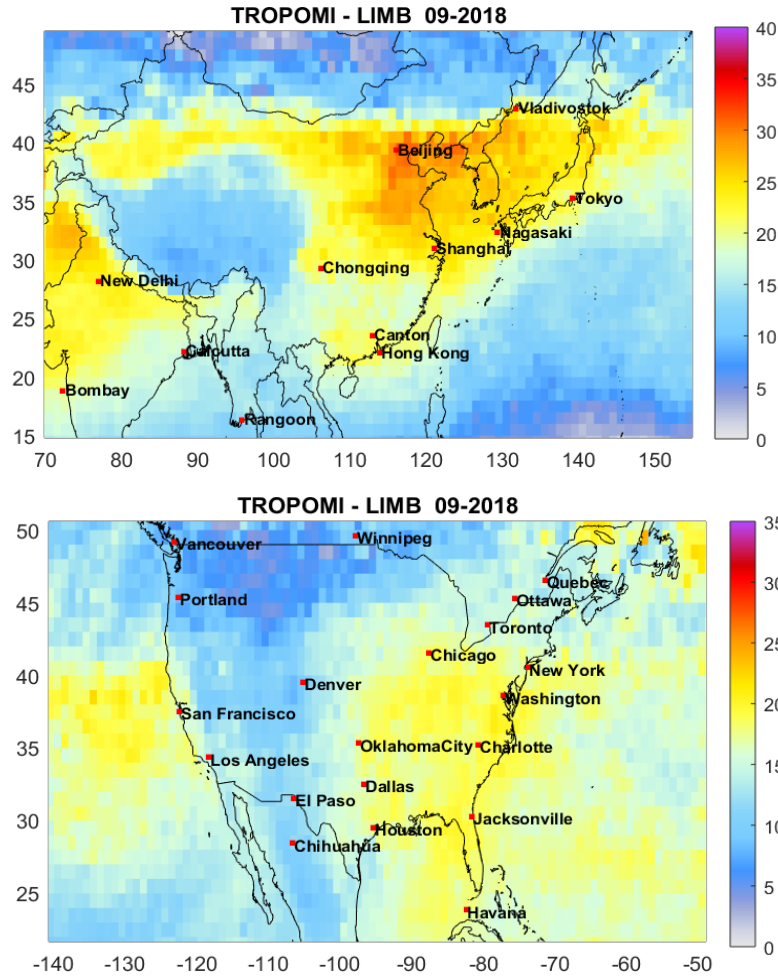


Figure 12. As Figure 11, but with zoom on China (top) and USA (bottom).

Uncertainties of daily tropospheric ozone values are estimated as:

$$\sigma_{TOC}^2 = \sigma_{TOC}^2 + \sigma_{SOC}^2 \cdot \quad (4)$$

The uncertainties of monthly average data are estimated similarly to uncertainties of gridded data, i.e., by Eq.(1).

## 5 A limited validation and examples of data

### 5.1 Comparisons of with ozone sondes

To assess the quality of high-resolution SUNLIT ozone profiles, we compared them with the ozonesonde data. For this comparison, we used the collection of ozonesonde data from the BDBP database (Hassler et al., 2008) in 2004-2006. In these comparisons, ozonesonde data are smoothed down to 1 km vertical resolution, and they are collocated with SUNLIT data within a day and 1° in latitude and longitude from the station location. The information

about the selected ozonesonde data is collected in Table 2. Several examples - for polar, tropical and mid-latitude stations, in winter and in summer - are shown in Figure 13.. As observed in this figure, ozonesonde and limb profiles – from both high-resolution satellite and SILAM-adjusted datasets - are in very good agreement.

The results of the statistics of differences (sonde minus satellite/model) for the selected stations - the median and 16<sup>th</sup> and 84<sup>th</sup> percentiles – are shown in Figure 14, for both interpolated limb profiles and adjusted SILAM data.

*Table 2. Information about ozone sonde data used in comparisons*

<b>Station name</b>	<b>Latitude</b>	<b>Longitude</b>	<b>Num. of collocations</b>	<b>Data sources</b>
<b>Eureka/ Eureka Lab</b>	80.04	-86.17	58	WOUDC
<b>Payerne</b>	46.49	6.57	165	WOUDC
<b>San Cristobal</b>	-0.92	-89.60	32	WOUDC & SHADOZ
<b>Irene</b>	-25.91	28.21	32	WOUDC
<b>Neumayer</b>	-70.65	-8.25	85	WOUDC
<b>Heredia</b>	10.00	-84.11	20	WOUDC & SHADOZ

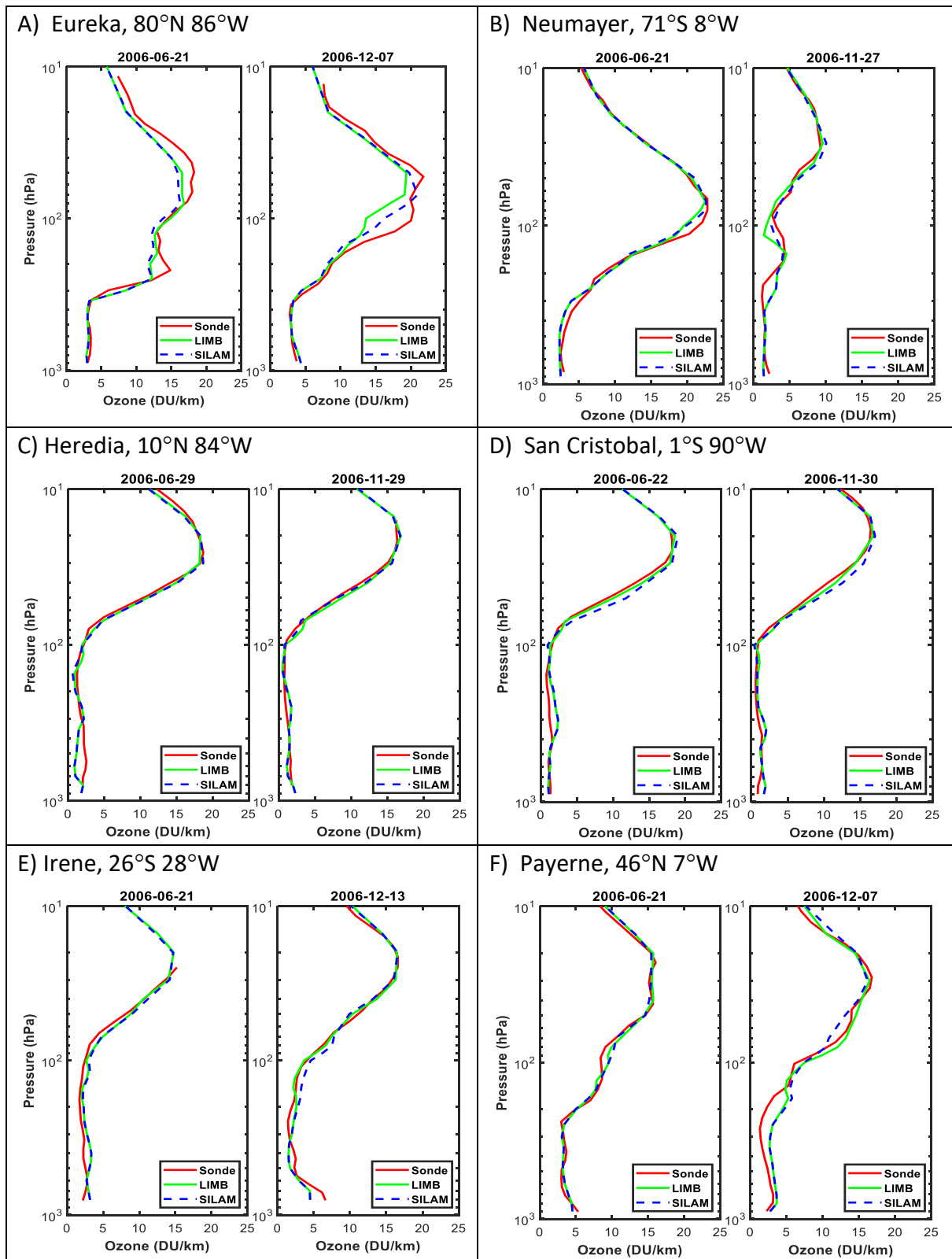


Figure 13. Several examples of ozonesonde data, high-resolution limb profiles and adjusted SILAM ozone profiles.

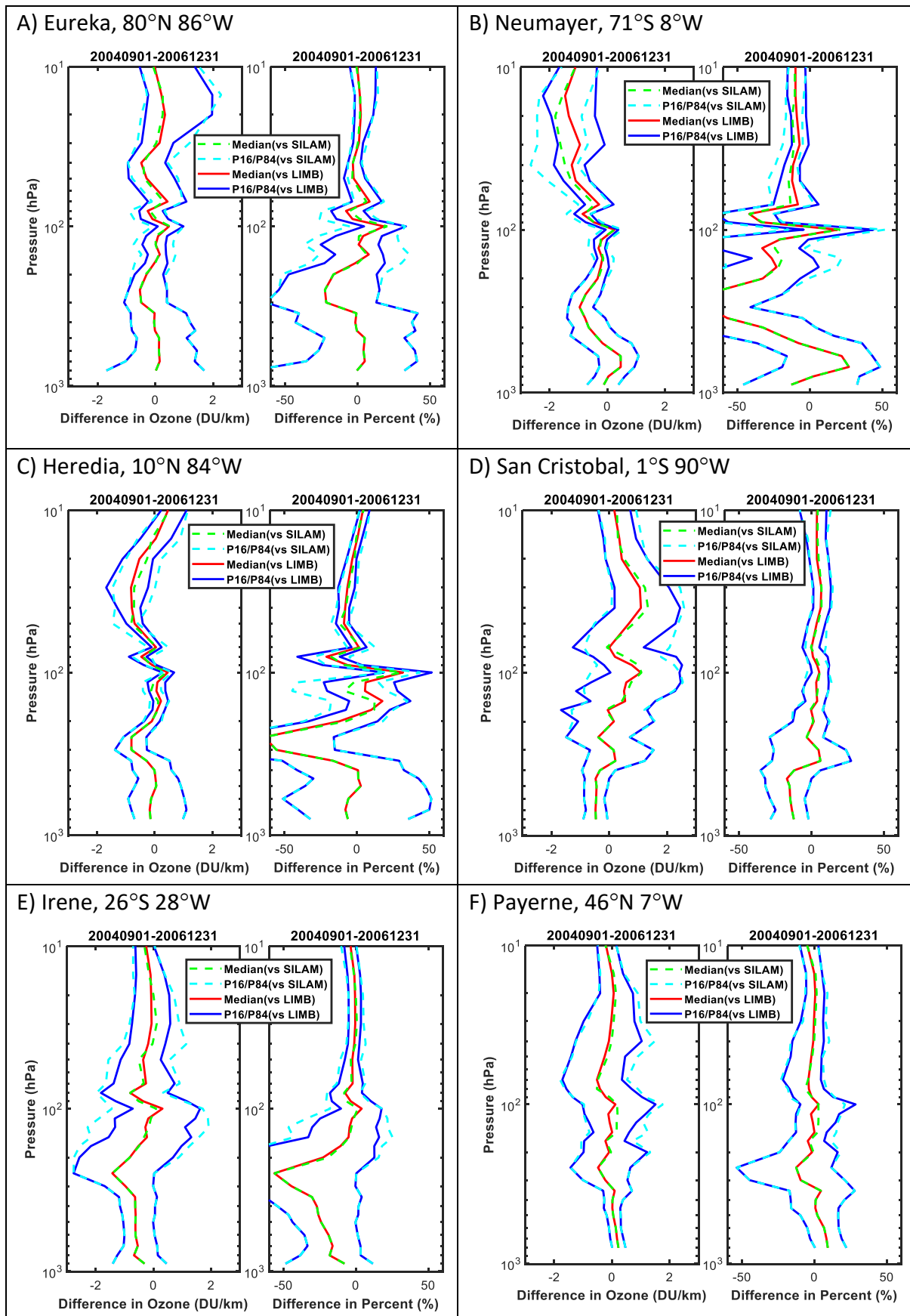


Figure 14. The statistical parameters of differences between ozonesonde and interpolated limb profiles (LIMB), and between ozonesonde and adjusted SILAM ozone profiles.

## 5.2 Comparison with OMI-MLS

For comparison with the NASA OMI-MLS tropospheric ozone column (obtained from [https://acd-ext.gsfc.nasa.gov/Data\\_services/cloud\\_slice/new\\_data.html](https://acd-ext.gsfc.nasa.gov/Data_services/cloud_slice/new_data.html)), we computed the stratospheric ozone column from the tropopause, as it is done in the OMI-MLS dataset. The examples of tropospheric ozone column for July 2008 are shown in Figure. 15.

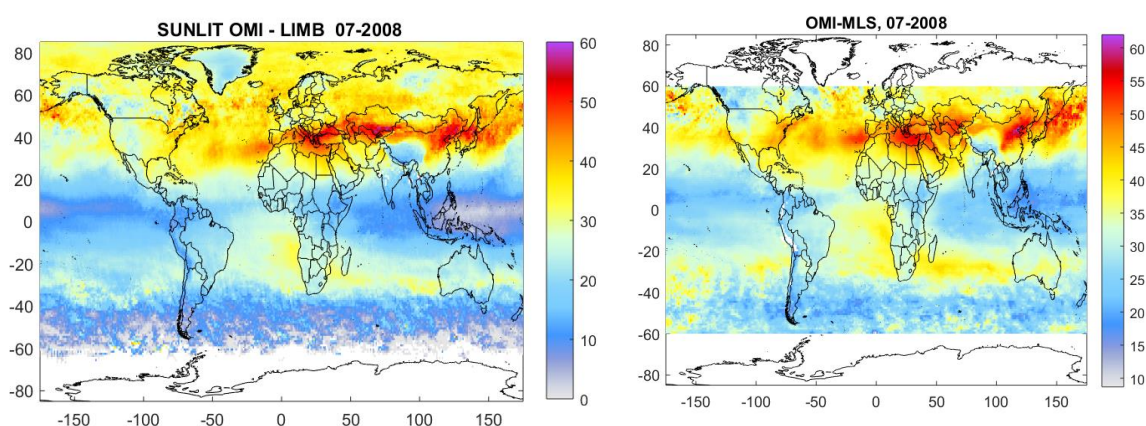


Figure. 15 Left: SUNLIT tropospheric ozone column for July 2008 (OMI minus limb SOC); right: NASA OMI-MLS tropospheric ozone column.

## 5.3 Comparison with CCD ozone

The convective cloud differential method (CCD) allows retrievals of tropospheric ozone column in the tropical region, at latitudes 20S-20N. The CCD tropospheric ozone dataset has been developed in ozone CCI project; it represents the ozone column in the altitude range from ground to 10 km. For comparison with the OMI CCD tropospheric ozone column, we integrated the limb ozone profiles from 10 km to 55 km, and subtracted it from clear-sky total ozone column. The comparison of tropospheric ozone columns from CCD method and from our computations are presented in Figure 16.

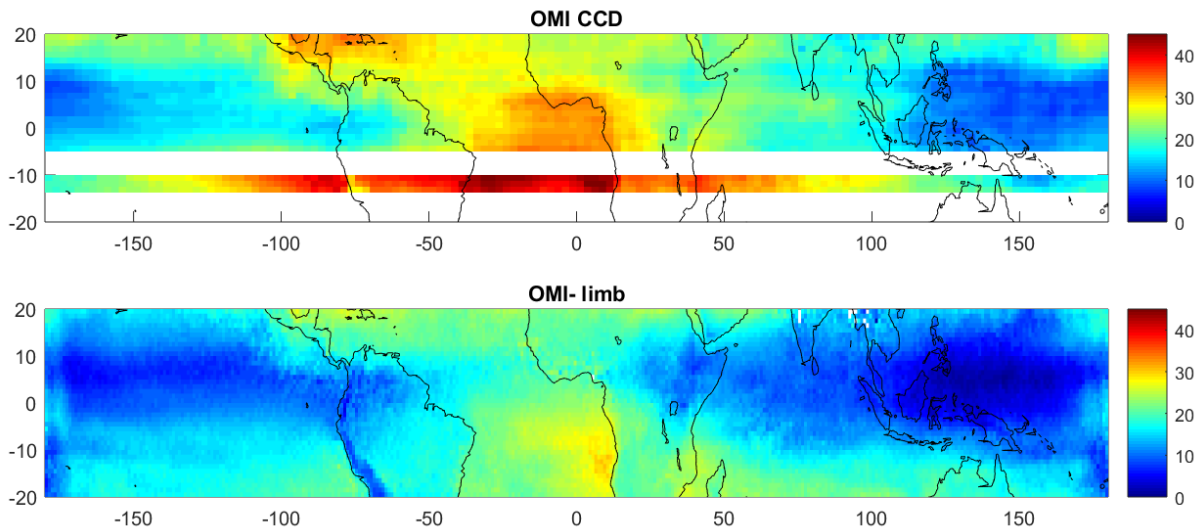


Figure 16. Tropospheric ozone column for July 2008 from OMI CCD (top) and SUNLIT data (SOC is integrated from 10 km).

## 6 Summary

In this TN, we have presented the results of our studies on the methods for retrievals of tropospheric ozone column by the residual method, i.e., the combination of total ozone column from nadir instruments with the stratospheric ozone column from limb instruments. The main result of the SUNLIT project is the tropospheric ozone column datasets obtained by combining the OMI and TROPOMI total-ozone columns with ozone profiles from the limb satellite instruments. The data are the monthly-averaged distributions with the horizontal resolution of  $1^{\circ} \times 1^{\circ}$ . The data are in open access at Sodankylä National Satellite Data centre [https://nsdc.fmi.fi/data/data\\_sunlit.php](https://nsdc.fmi.fi/data/data_sunlit.php).

Other datasets, which are created as an intermediate step of creating the tropospheric ozone column data, have their own value. These datasets are daily gridded with  $1^{\circ} \times 1^{\circ}$  horizontal resolution and include (i) homogenized and interpolated dataset of ozone profiles from limb instruments, (ii) stratospheric ozone column from limb instruments, and (iii) clear-sky and total ozone columns from nadir instruments.

Several methodological developments are made in the project. These include: (a) method for horizontal interpolation, which takes into account both data uncertainties and variability of the parameter of interest, (b) application of the structure function method for validation probing small-scale natural variability and validation of random uncertainties in the data (Sofieva et al., 2020).

Using simulations with the chemistry-transport model SILAM, we have investigated the possibilities and the limitations of the residual method. During the project, the SILAM ozone data have been extensively compared with the satellite data. Several important modifications have been introduced into the model, which include: correction of natural NO<sub>x</sub> emission in

the tropics, changes in chemistry and photolysis schemes, and a new scavenging scheme. As a result of these modifications, the ozone field in the updated SILAM simulations is significantly closer to observations than it was in the beginning of the SUNLIT project.

## 7 Supplementary material

### 7.1 Feasibility studies on residual method to retrieve tropospheric ozone

The feasibility studies on tropospheric ozone retrievals using the residual method are performed using of the full SILAM ozone field.

The effect of the upper stratospheric ozone column correction using the tropopause-related ozone climatology is illustrated in Figure S1.

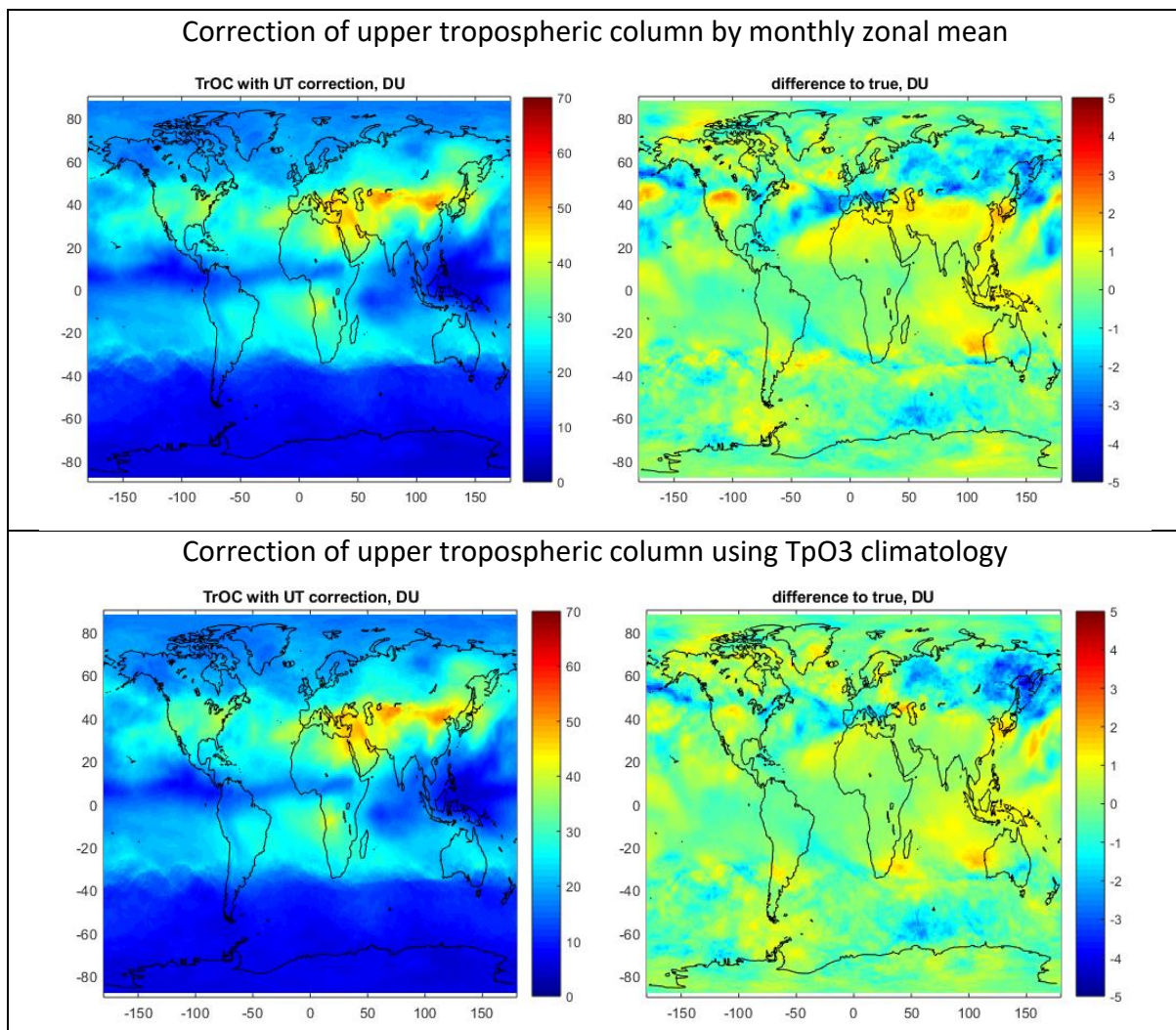


Figure S1. Illustration of correction by UT when the upper tropospheric ozone is estimated using monthly mean values (top) and using the tropopause-related ozone climatology (bottom). Left panels: estimated truncated TrOC for July 2008, right: difference to true truncated TrOC.

Figure S2 compares the monthly average tropospheric ozone column  $\langle \text{TrOC} \rangle$  for July 2008 from the full SILAM field (left), the TrOC computed as  $\langle \text{TrOC} \rangle = \langle \text{TOC} \rangle - \langle \text{SOC} \rangle$  (right) and the TrOC computed using the daily data  $\langle \text{TrOC} \rangle = \langle \text{TOC} - \text{SOC} \rangle$  (center). As observed in Figure S2, tropospheric column computed via averaging daily TrOC data are much closer to the true distribution than computed via averaging first SOC data.

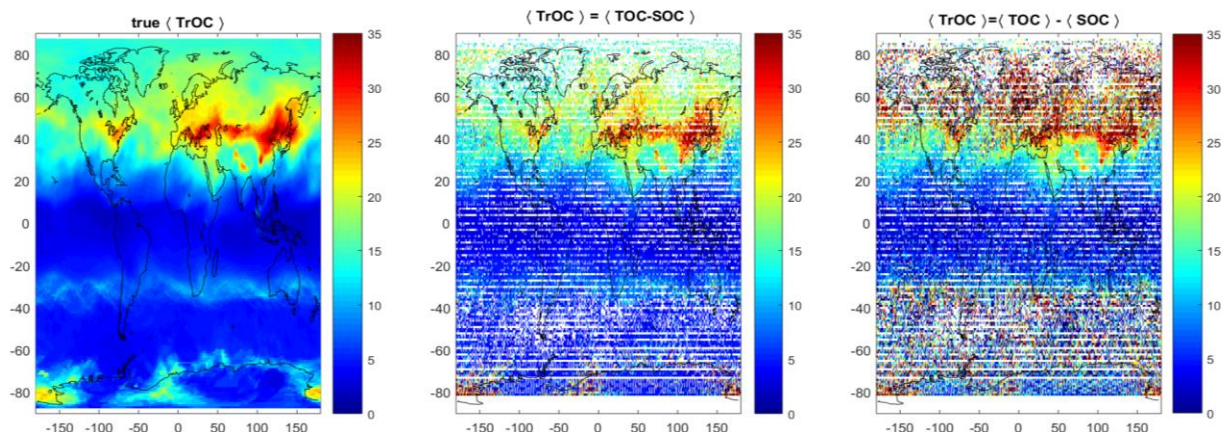


Figure S2. “True” monthly average tropospheric ozone column  $\langle \text{TrOC} \rangle$  for July 2008 from the full SILAM field (left),  $\langle \text{TrOC} \rangle = \langle \text{TOC} \rangle - \langle \text{SOC} \rangle$  (right), and the TrOC computed using the daily data  $\langle \text{TrOC} \rangle = \langle \text{TOC} - \text{SOC} \rangle$  (center).

Typical averaging kernels for OMI and TROPOMI are shown in Figure S3.

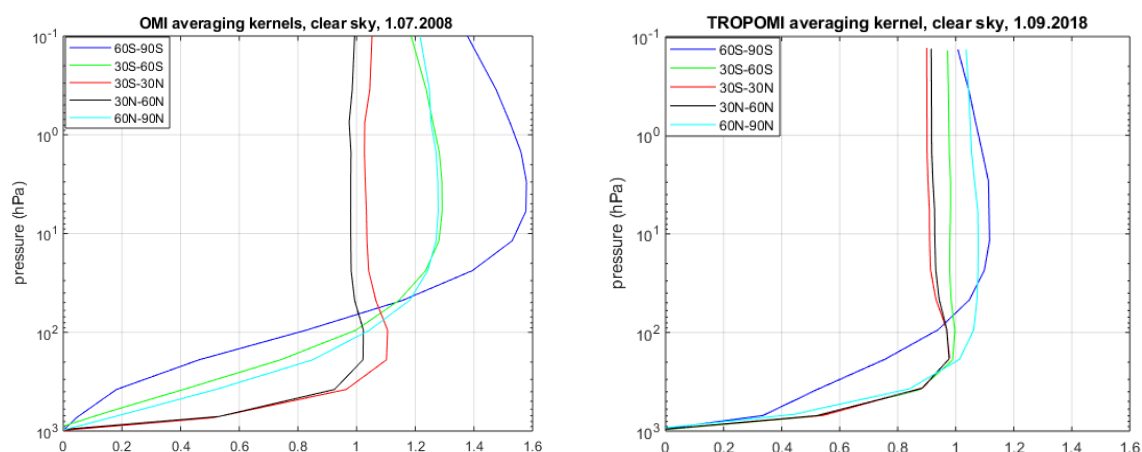


Figure S3. Left: typical OMI averaging kernels for clear-sky conditions (example for 1 July 2008). Right: TROPOMI typical averaging kernels for clear-sky conditions (example for 1 September 2018).

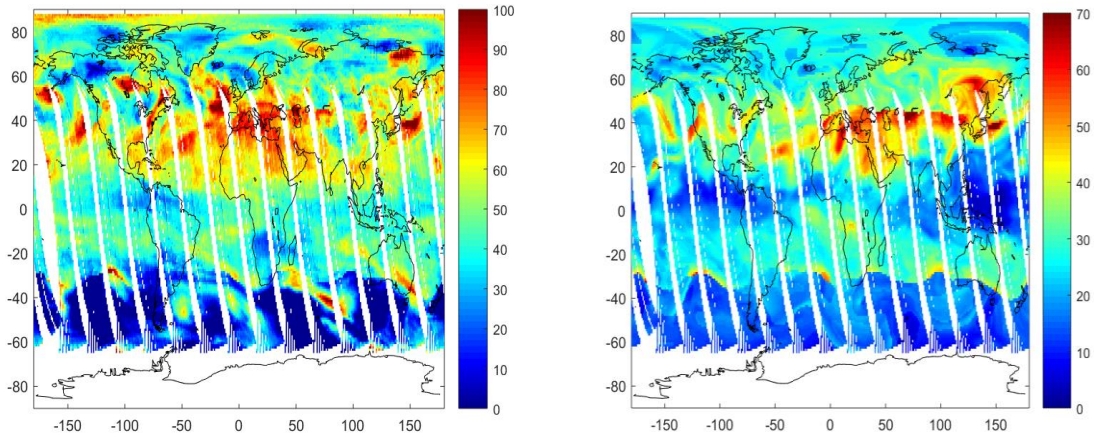


Figure S4. Tropospheric ozone column (from ground to tropopause) 1 July 2008 evaluated using SILAM data. Left – in OMI local time, right – daily mean (at OMI locations).

## 7.2 Adjusted SILAM ozone field

The simulated ozone field by the chemistry-transport model is an attractive source of information. This additional source of information is of especial importance in the UTLS, where the accuracy of satellite data is rather poor and the covered altitude range is not uniform over the globe, and it is instrument-specific, thus the resulting field based on data solely may be not accurate.

The SILAM model is proved to produce realistically distribution of ozone field, including the special events like ozone hole and mini-holes (Sofiev et al., 2020), <https://en.ilmatietaenlaitos.fi/news/1140594517>; <https://en.ilmatietaenlaitos.fi/tiedote/1276664372>). In addition, we have studied the small-scale ozone variability by the structure function method using OMI and SILAM total ozone column data and have found that they are in a very good agreement (Supplement, Sect S3). However, the model field is biased with respect to satellite data.

One possible approach to make the model data consistent with observations is data assimilation. The main problem with the assimilated data is their sensitivity to the amount of data used for assimilation, which can affect the long-term stability of the assimilated data. We apply a different approach: we adjust SILAM data to MLS observation by computing daily biases. These biases are evaluated as a weighted mean of model deviations from the observations in  $10^\circ \times 30^\circ$  latitude-longitude bin, for each pressure level and each grid-point. As an example, MLS observations, original SILAM data, and the adjusted SILAM data for 20 June 2018 are shown in Figure S5.

The size of latitude-longitude box for evaluation of SILAM bias is relatively large, so that the small-scale structure of the model field is preserved in the adjusted field. For example, one can notice interesting small-scale perturbations in Figure S5.

The uncertainty associated with the bias correction is estimated as the interpolated absolute difference between MLS and SILAM adjusted data. In majority of location, the estimated uncertainty is a few percent (an example is shown in Figure S5, right bottom panel).

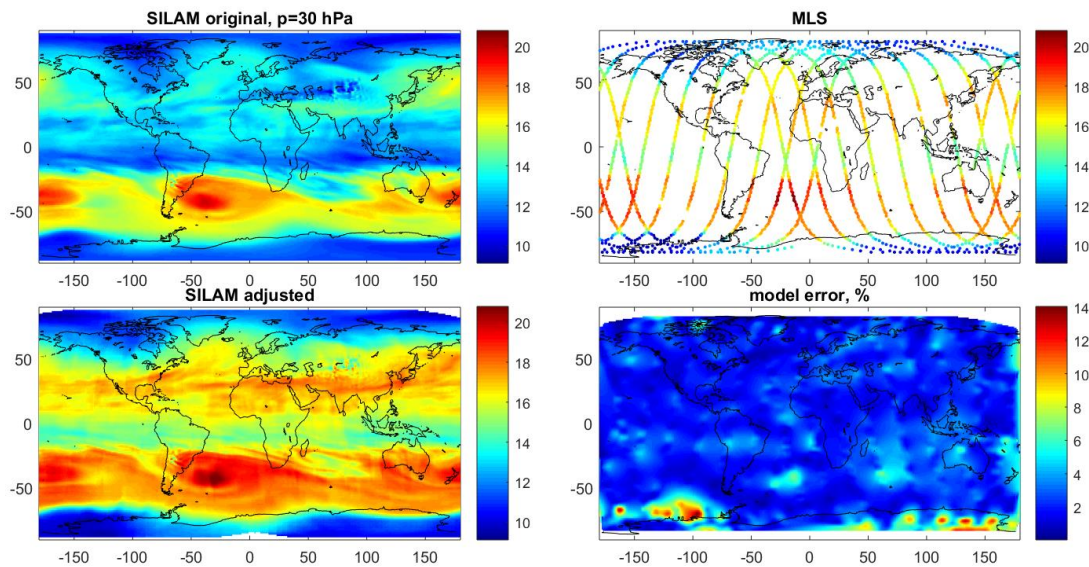


Figure S5. Ozone (DU/km) at 30 hPa on 20 June 2018 from original SILAM data (left top), MLS observation (right top), adjusted SILAM data (left bottom). The uncertainties associated with adjusted SILAM data are shown on right bottom panel.

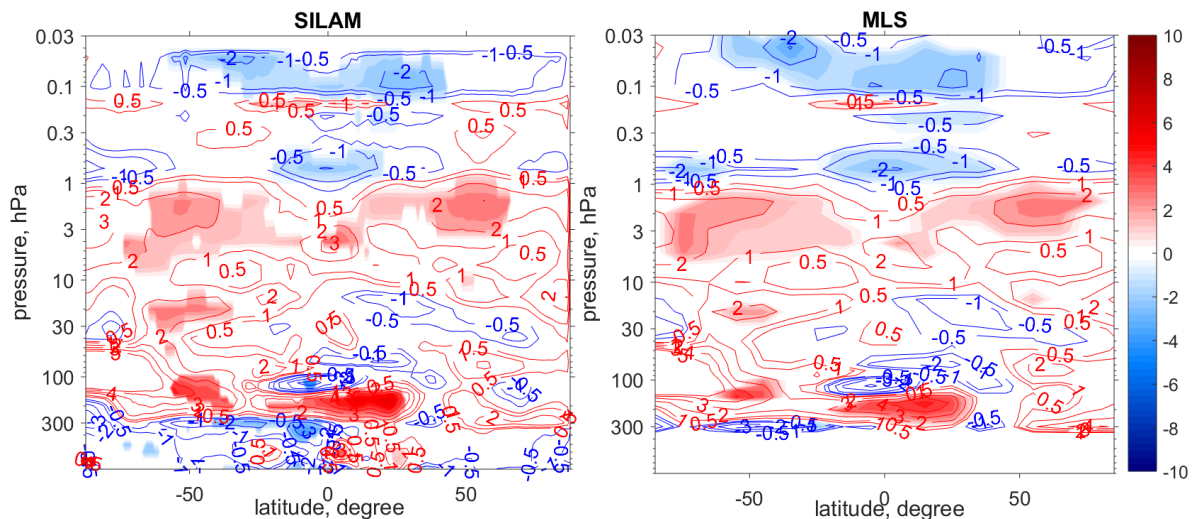


Figure S6. Ozone trends(% dec<sup>-1</sup>) in 2004-2018 on as a function of latitude and altitude. Ozone trends are evaluated via multiple linear regression (Sofieva et al., 2017; 2020b) using adjusted SILAM ozone profiles (left) and MLS data (right). All trends are shown by colored contours, while the statistically significant at 95% level trends are shown by filled contours.

Contrary to assimilation, the model is “fixed” to observations, so that the potentially wrong trends in a model does not affect the resulting dataset. This is illustrated in Figure S6, which

compares the zonal mean ozone trends in 2004-2018 from MLS and from adjusted SILAM dataset. As observed in Figure S6, these trends are nearly identical.

Since MLS profiles are recommended for use at altitudes above 250 hPa, we apply a fast 3-point linear transition to original SILAM ozone profiles at lower altitudes: at 250 hPa, the adjusted model is used, at next level below (300 hPa) – the mean of original and adjusted data, and 350 hPa and below – original SILAM data.

### 7.3 Analyses of small-scale ozone variability using OMI and SILAM data

For the analyses, we used SILAM simulated ozone field and OMI data. For SILAM, we used daily average data. For selection of tropospheric and stratospheric ozone columns, we used the thermal tropopause/ozonopause definition as described above. For OMI, the daily gridded data  $1^\circ \times 1^\circ$  are used. Stratospheric ozone column corresponds to the cloudy conditions, i.e. we used columns where clouds overshadowed the tropospheric part.

All ozone columns - total, stratospheric and tropospheric - have large temporal variability. Analogously to (Sofieva et al., 2020), we will characterize the variability of the ozone field by the structure function [e.g., *Tatarskii, 1961*]:

$$D(\boldsymbol{\rho}) = D(\mathbf{r}_1 - \mathbf{r}_2) = \left\langle [f(\mathbf{r}_1) - f(\mathbf{r}_2)]^2 \right\rangle, \quad (5)$$

where  $\mathbf{r}_1$  and  $\mathbf{r}_2$  are two locations and  $\boldsymbol{\rho} = \mathbf{r}_1 - \mathbf{r}_2$ . This concept assumes that the random field is locally homogeneous, which is the spatial equivalence of a random process with stationary increments. In spatial statistics,  $D(\boldsymbol{\rho})$  is called the variogram (Wackernagel, 2003).

The structure functions in latitude and in longitude are evaluated for different seasons and broad latitude bands for years 2005-2017, for both total and stratospheric columns and experimental and simulated ozone fields. The TOC structure functions are shown in Figures S7 and S8, for OMI and SILAM data, respectively. The analogous structure functions for SOC are shown in Figures S9 and S10.

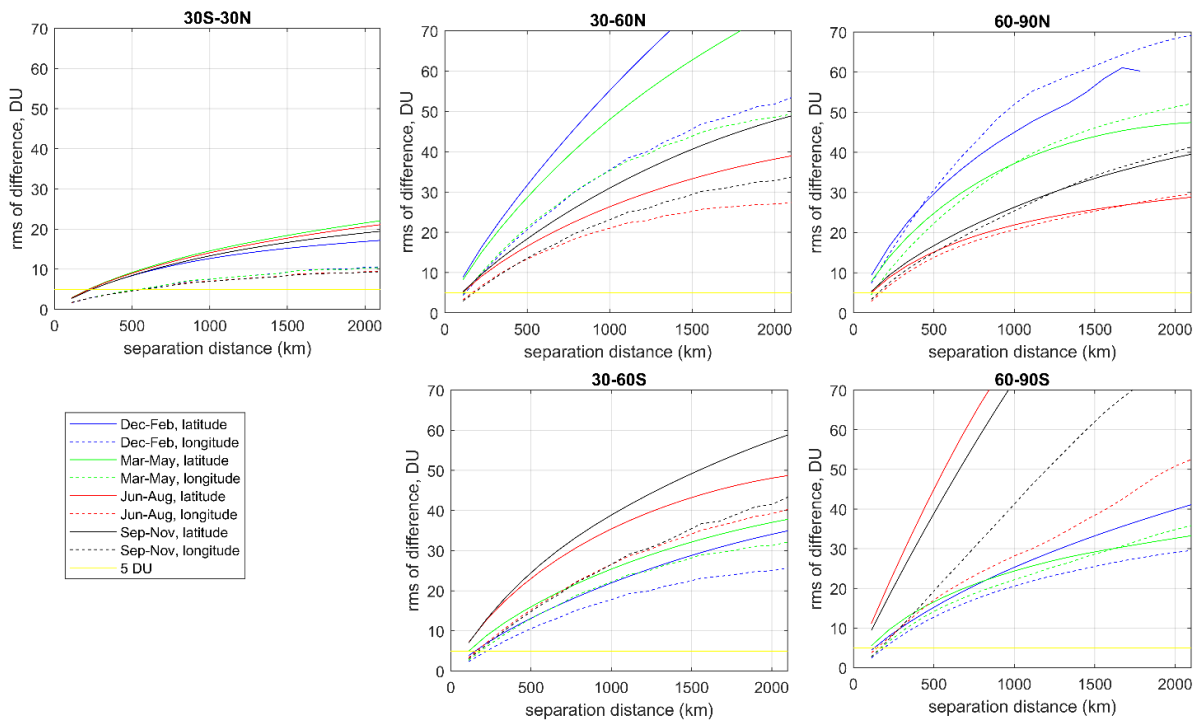


Figure S7. OMI TOC structure function, for different latitude bands and seasons. The horizontal yellow line corresponds to level 5 DU.

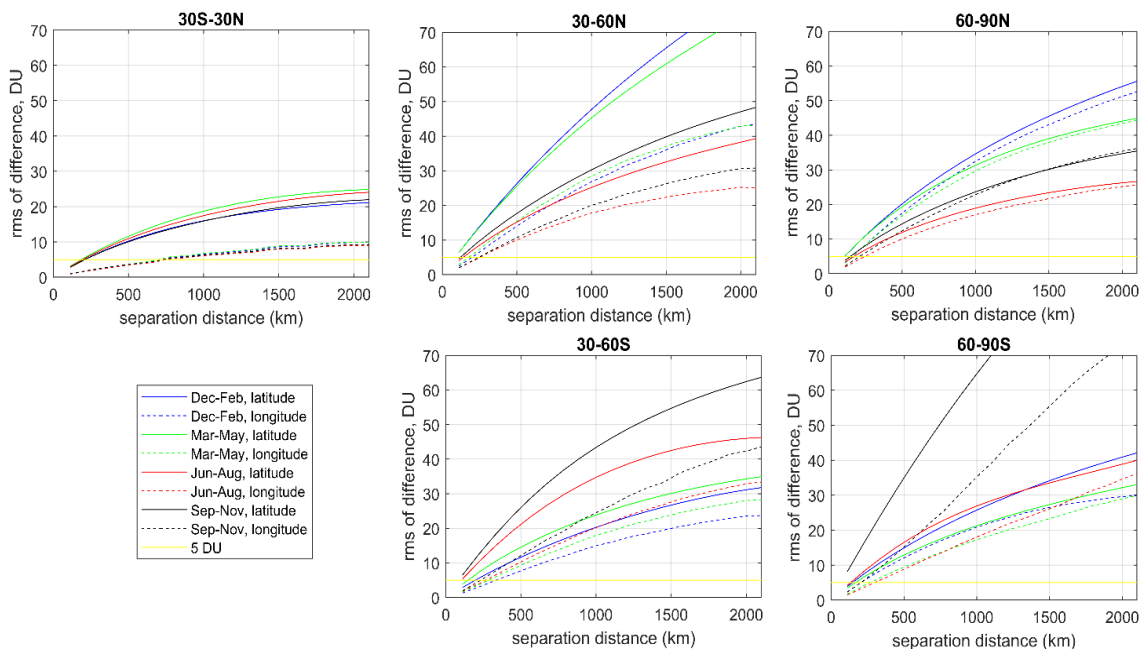


Figure S8. As Figure S6, but for SILAM TOC.

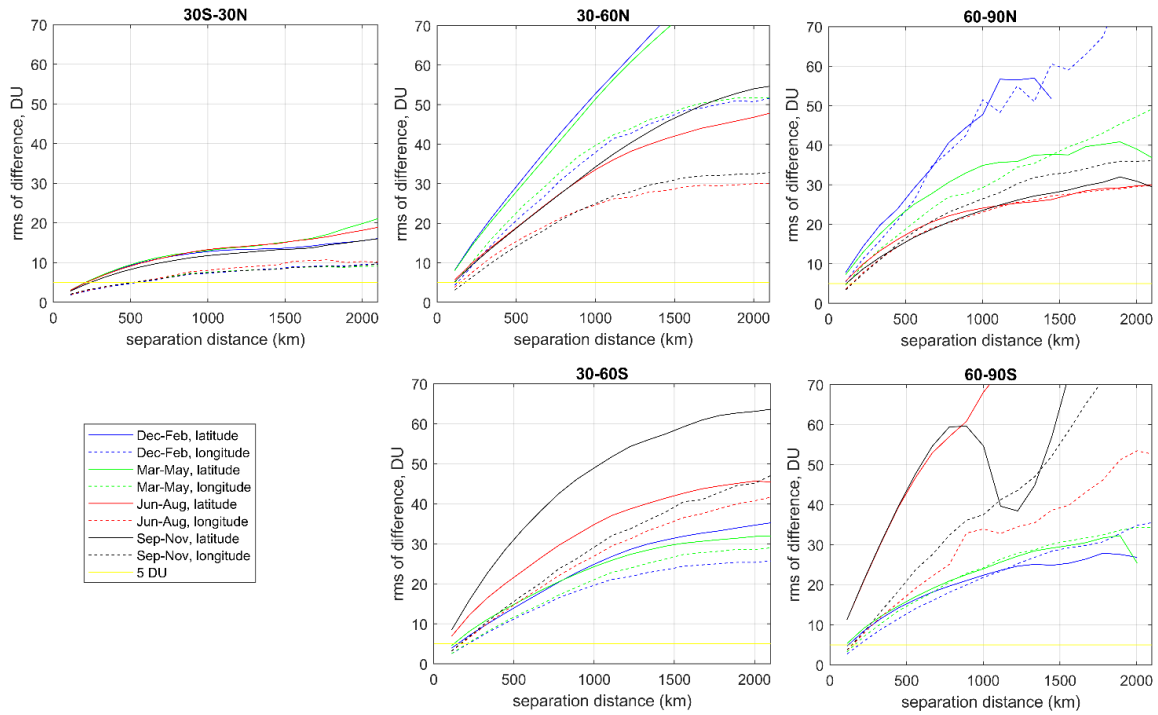


Figure S9. As Figure S6, but for SOC using OMI data.

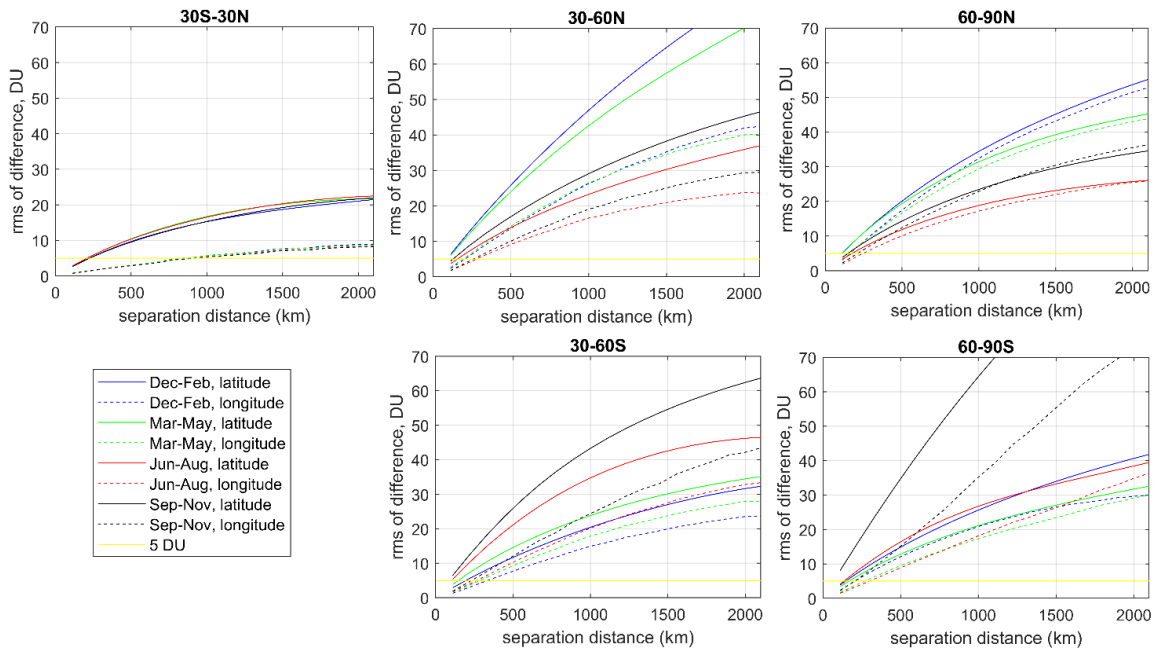


Figure S10 As Figure S6, but for SOC using SILAM data.

The obtained morphology of ozone variability is quite expected: it is overall much smaller in the tropics than at middle and high latitudes, where it has a pronounced seasonal cycle. In polar regions in winter and spring the ozone variability is very strong, even for small separations. The structure functions are evidently anisotropic nearly everywhere, with stronger variability in latitudinal direction. The only exceptions are latitudes 60-90 N in all

seasons and 60-90 S in March-May. As expected, the structure functions for total ozone and for stratospheric ozone look similar. The modelled and experimental data are in a very good agreement.

#### 7.4 Uncertainties of the interpolated ozone profiles

The estimation of uncertainties associated with the interpolated dataset of ozone profiles are illustrated in Figure S11. First, we used error propagation to evaluate uncertainty after the kriging (Figure S11, top right). In addition, we estimated the interpolation uncertainty using the SILAM data: we run the same interpolation but on SILAM sub-sampled in measurements location, and evaluated the error as the absolute difference of true and interpolated data (Figure S11, bottom left). The final uncertainty is the root-mean-square of error propagation and model-assessed interpolation errors (Figure S11, bottom right).

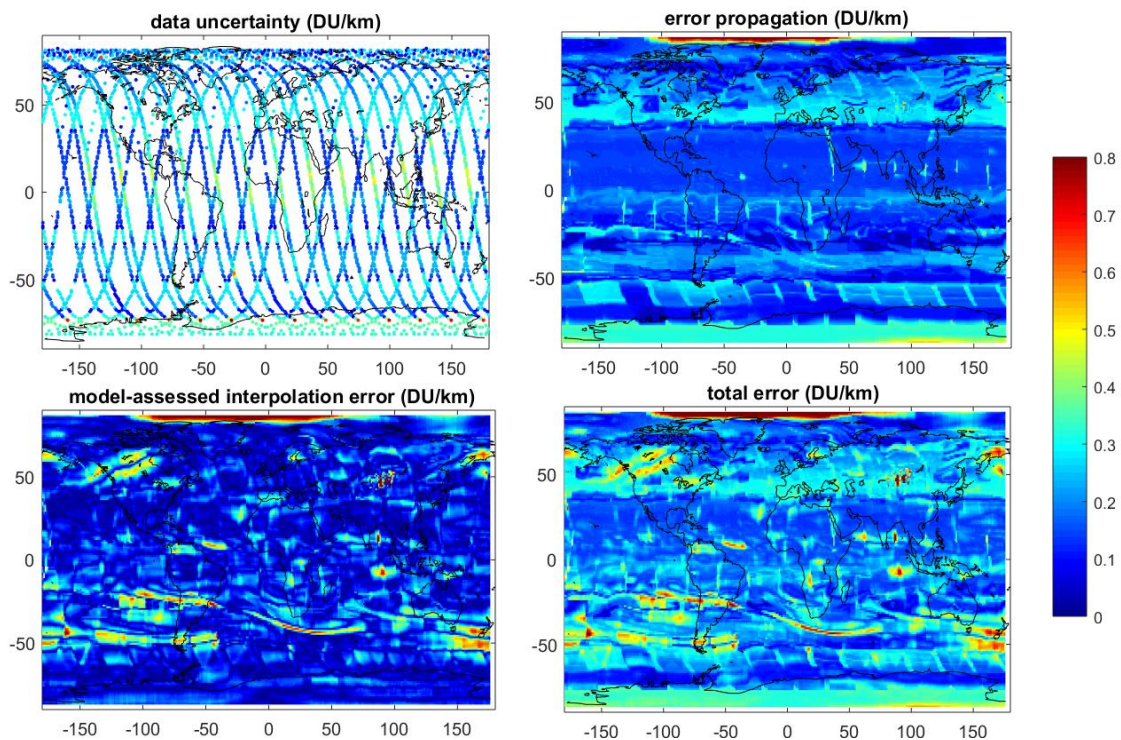


Figure S11. Illustration of uncertainty estimation of the interpolated ozone data. Data are for 1 Sep 2018, at 10 hPa. Top left: uncertainty of satellite data, top right: error propagation after kriging-type interpolation, bottom left: interpolation error from SILAM data, bottom left: total uncertainty.

## 7.5 Compatibility of ozone data from limb and nadir instruments.

We compared OMI and TROPOMI measurements in cloudy conditions (the ghost column is removed) with the integrated ozone profiles from the cloud-top height. For this comparison, we selected cloudy pixels with cloud fraction  $>0.8$  and cloud-top pressure less than 350 hPa and the corresponding limb profiles from SILAM adjusted field. The example comparison for September 2018 is shown in Figure S12.

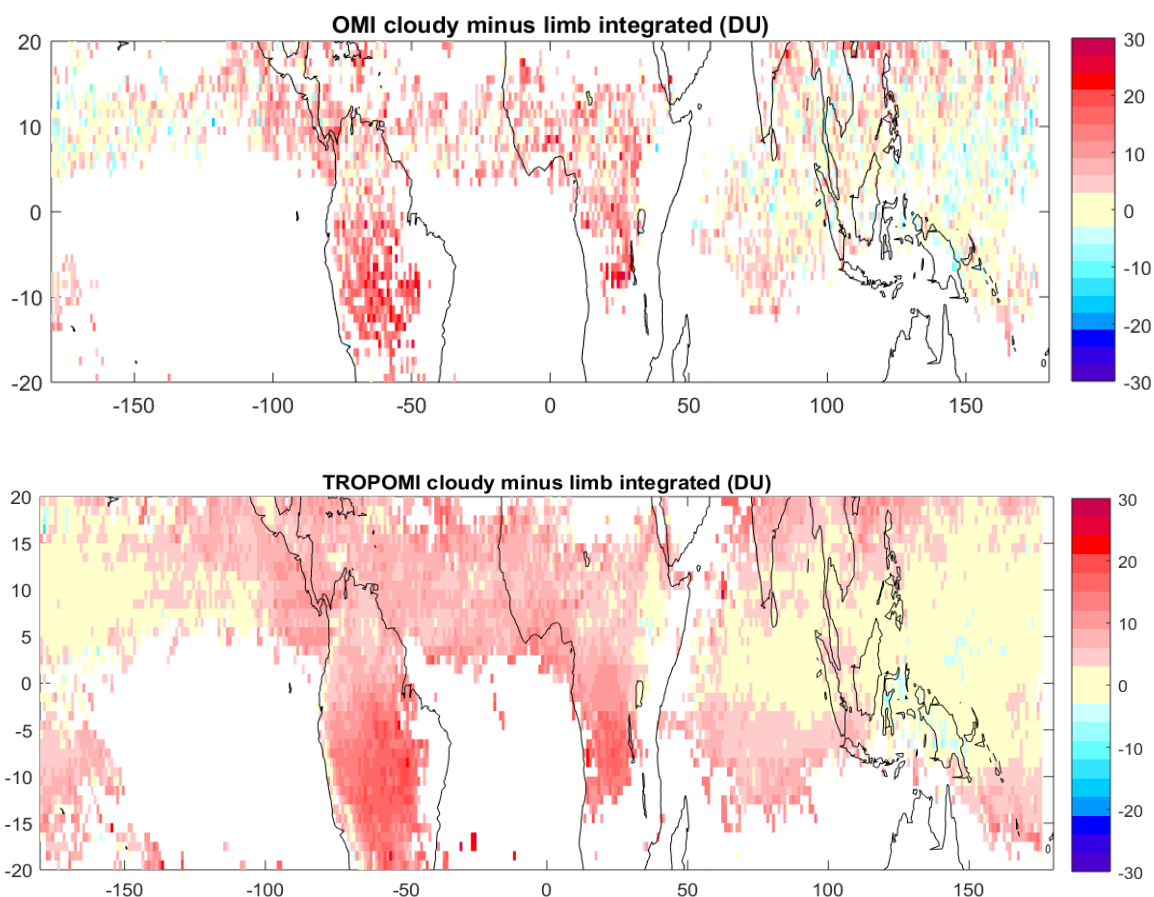


Figure S12. Total column in cloudy pixels from nadir instruments minus adjusted SILAM integrated from the cloud-top height, Sep 2018. Top: OMI, bottom: TROPOMI.

## 8 References

Brasseur, G. P., Xie, Y., Petersen, A. K., Bouarar, I., Flemming, J., Gauss, M., Jiang, F., Kouznetsov, R., Kranenburg, R., Mijling, B., Peuch, V.-H., Pommier, M., Segers, A., Sofiev, M., Timmermans, R., van der A, R., Walters, S., Xu, J. and Zhou, G.: Ensemble forecasts of air quality in eastern China -- Part 1: Model description and implementation of the MarcoPolo--Panda prediction system, version 1, *Geosci. Model Dev.*, 12(1), 33–67, doi:10.5194/gmd-12-33-2019, 2019.

Ebojje, F., Burrows, J. P., Gebhardt, C., Ladstätter-Weißenmayer, A., von Savigny, C.,

Rozanov, A., Weber, M. and Bovensmann, H.: Global tropospheric ozone variations from 2003 to 2011 as seen by SCIAMACHY, *Atmos. Chem. Phys.*, 16(2), 417–436, doi:10.5194/acp-16-417-2016, 2016.

Fishman, J. and Larsen, J. C.: Distribution of total ozone and stratospheric ozone in the tropics: Implications for the distribution of tropospheric ozone, *J. Geophys. Res. Atmos.*, 92(D6), 6627–6634, doi:10.1029/JD092iD06p06627, 1987.

Fishman, J., Watson, C. E., Larsen, J. C. and Logan, J. A.: Distribution of tropospheric ozone determined from satellite data, *J. Geophys. Res.*, 95, 3599–3617, 1990.

Gery, M. W., Whitten, G. Z., Killus, J. P. and Dodge, M. C.: A photochemical kinetics mechanism for urban and regional scale computer modeling, *J. Geophys. Res.*, 94(12), 12925–12956, 1989.

Hassler, B., Bodeker, G. E. and Dameris, M.: Technical Note: A new global database of trace gases and aerosols from multiple sources of high vertical resolution measurements, *Atmos. Chem. Phys.*, 8(17), 5403–5421, doi:10.5194/acp-8-5403-2008, 2008.

Jacobson, M. Z.: *Air Pollution and Global Warming: History, Science, and Solutions*, 2nd ed., Cambridge University Press, Cambridge, UK., 2012.

Korhonen, A., Lehtomäki, H., Rumrich, I., Karvosenoja, N., Paunu, V.-V., Kupiainen, K., Sofiev, M., Palamarchuk, Y., Kukkonen, J., Kangas, L., Karppinen, A. and Hänninen, O.: Influence of spatial resolution on population PM<sub>2.5</sub> exposure and health impacts, *Air Qual. Atmos. Heal.*, 12(6), 705–718, doi:10.1007/s11869-019-00690-z, 2019.

Kouznetsov, R. and Sofiev, M.: A methodology for evaluation of vertical dispersion and dry deposition of atmospheric aerosols, *J. Geophys. Res. Atmos.*, 117(D1), doi:https://doi.org/10.1029/2011JD016366, 2012.

Kouznetsov, R., Sofiev, M., Vira, J. and Stiller, G.: Simulating age of air and the distribution of  $\text{SF}_6$  in the stratosphere with the SILAM model, *Atmos. Chem. Phys.*, 20(9), 5837–5859, doi:10.5194/acp-20-5837-2020, 2020.

Kroon, M., de Haan, J. F., Veefkind, J. P., Froidevaux, L., Wang, R., Kivi, R. and Hakkarainen, J. J.: Validation of operational ozone profiles from the Ozone Monitoring Instrument, *J. Geophys. Res.*, 116(D18), D18305, doi:10.1029/2010JD015100, 2011.

Kukkonen, J., Olsson, T., Schultz, D. M., Baklanov, A., Klein, T., Miranda, A. I., Monteiro, A., Hirtl, M., Tarvainen, V., Boy, M., Peuch, V.-H., Poupkou, A., Kioutsioukis, I., Finardi, S., Sofiev, M., Sokhi, R., Lehtinen, K. E. J., Karatzas, K., San José, R., Astitha, M., Kallos, G., Schaap, M., Reimer, E., Jakobs, H. and Eben, K.: A review of operational, regional-scale, chemical weather forecasting models in Europe, *Atmos. Chem. Phys.*, 12(1), 1–87, doi:10.5194/acp-12-1-2012, 2012.

Lerot, C., Van Roozendaal, M., Spurr, R., Loyola, D., Coldewey-Egbers, M., Kochenova, S., van Gent, J., Koukouli, M., Balis, D., Lambert, J.-C., Granville, J. and Zehner, C.: Homogenized total ozone data records from the European sensors GOME/ERS-2, SCIAMACHY/Envisat, and GOME-2/MetOp-A, *J. Geophys. Res. Atmos.*, 119(3), 1639–1662, doi:10.1002/2013JD020831, 2014.

Levelt, P. F., Joiner, J., Tamminen, J., Veefkind, J. P., Bhartia, P. K., Stein Zweers, D. C.,

Duncan, B. N., Streets, D. G., Eskes, H., van der A, R., McLinden, C., Fioletov, V., Carn, S., de Laat, J., DeLand, M., Marchenko, S., McPeters, R., Ziemke, J., Fu, D., Liu, X., Pickering, K., Apituley, A., González Abad, G., Arola, A., Boersma, F., Chan Miller, C., Chance, K., de Graaf, M., Hakkarainen, J., Hassinen, S., Ialongo, I., Kleipool, Q., Krotkov, N., Li, C., Lamsal, L., Newman, P., Nowlan, C., Suleiman, R., Tilstra, L. G., Torres, O., Wang, H. and Wargan, K.: The Ozone Monitoring Instrument: overview of 14 years in space, *Atmos. Chem. Phys.*, 18(8), 5699–5745, doi:10.5194/acp-18-5699-2018, 2018.

Lippmann, M.: Health effects of tropospheric ozone, *Environ. Sci. Technol.*, 25(12), 1954–1962, doi:10.1021/es00024a001, 1991.

Liu, X., Bhartia, P. K., Chance, K., Spurr, R. J. D. and Kurosu, T. P.: Ozone profile retrievals from the Ozone Monitoring Instrument, *Atmos. Chem. Phys.*, 10(5), 2521–2537, doi:10.5194/acp-10-2521-2010, 2010a.

Liu, X., Bhartia, P. K., Chance, K., Froidevaux, L., Spurr, R. J. D. and Kurosu, T. P.: Validation of Ozone Monitoring Instrument (OMI) ozone profiles and stratospheric ozone columns with Microwave Limb Sounder (MLS) measurements, *Atmos. Chem. Phys.*, 10(5), 2539–2549, doi:10.5194/acp-10-2539-2010, 2010b.

Marenco, A., Gouget, H., Nédélec, P., Pagés, J.-P. and Karcher, F.: Evidence of a long-term increase in tropospheric ozone from Pic du Midi data series: Consequences: Positive radiative forcing, *J. Geophys. Res. Atmos.*, 99(D8), 16617–16632, doi:10.1029/94JD00021, 1994.

Mielonen, T., de Haan, J. F., van Peet, J. C. A., Eremenko, M. and Veefkind, J. P.: Towards the retrieval of tropospheric ozone with the Ozone Monitoring Instrument (OMI), *Atmos. Meas. Tech.*, 8(2), 671–687, doi:10.5194/amt-8-671-2015, 2015.

Petersen, A. K., Brasseur, G. P., Bouarar, I., Flemming, J., Gauss, M., Jiang, F., Kouznetsov, R., Kranenburg, R., Mijling, B., Peuch, V.-H., Pommier, M., Segers, A., Sofiev, M., Timmermans, R., van der A, R., Walters, S., Xie, Y., Xu, J. and Zhou, G.: Ensemble forecasts of air quality in eastern China -- Part 2: Evaluation of the MarcoPolo--Panda prediction system, version 1, *Geosci. Model Dev.*, 12(3), 1241–1266, doi:10.5194/gmd-12-1241-2019, 2019.

Schoeberl, M. R., Ziemke, J. R., Bojkov, B., Livesey, N., Duncan, B., Strahan, S., Froidevaux, L., Kulawik, S., Bhartia, P. K., Chandra, S., Levelt, P. F., Witte, J. C., Thompson, A. M., Cuevas, E., Redondas, A., Tarasick, D. W., Davies, J., Bodeker, G., Hansen, G., Johnson, B. J., Oltmans, S. J., Vömel, H., Allaart, M., Kelder, H., Newchurch, M., Godin-Beekmann, S., Ancellet, G., Claude, H., Andersen, S. B., Kyrö, E., Parrondos, M., Yela, M., Zabolocki, G., Moore, D., Dier, H., von der Gathen, P., Viatte, P., Stübi, R., Calpini, B., Skrivankova, P., Dorokhov, V., de Backer, H., Schmidlin, F. J., Coetzee, G., Fujiwara, M., Thouret, V., Posny, F., Morris, G., Merrill, J., Leong, C. P., Koenig-Langlo, G. and Joseph, E.: A trajectory-based estimate of the tropospheric ozone column using the residual method, *J. Geophys. Res. Atmos.*, 112(D24), n/a--n/a, doi:10.1029/2007JD008773, 2007.

Shindell, D., Faluvegi, G., Lacis, A., Hansen, J., Ruedy, R. and Aguilar, E.: Role of tropospheric ozone increases in 20th-century climate change, *J. Geophys. Res. Atmos.*, 111(D8), n/a--n/a, doi:10.1029/2005JD006348, 2006.

Sofiev, M.: Extended resistance analogy for construction of the vertical diffusion scheme for

dispersion models, *J. Geophys. Res. Atmos.*, 107(D12), ACH 10-1-ACH 10-8, doi:<https://doi.org/10.1029/2001JD001233>, 2002.

Sofiev, M.: On possibilities of assimilation of near-real-time pollen data by atmospheric composition models, *Aerobiologia (Bologna)*, 1, doi:10.1007/s10453-019-09583-1, 2019.

Sofiev, M., Vira, J., Kouznetsov, R., Prank, M., Soares, J. and Genikhovich, E.: Construction of an Eulerian atmospheric dispersion model based on the advection algorithm of M. Galperin: dynamic cores v.4 and 5 of SILAM v.5.5, *Geosci. Model Dev. Discuss.*, 8(3), 2905–2947, doi:10.5194/gmdd-8-2905-2015, 2015.

Sofiev, M., Winebrake, J. J., Johansson, L., Carr, E. W., Prank, M., Soares, J., Vira, J., Kouznetsov, R., Jalkanen, J.-P. and Corbett, J. J.: Cleaner fuels for ships provide public health benefits with climate tradeoffs, *Nat. Commun.*, 9(1), 406, doi:10.1038/s41467-017-02774-9, 2018.

Sofiev, M., Kouznetsov, R., Hänninen, R. and Sofieva, V. F.: Technical note: Intermittent reduction of the stratospheric ozone over northern Europe caused by a storm in the Atlantic Ocean, *Atmos. Chem. Phys.*, 20(3), 1839–1847, doi:10.5194/acp-20-1839-2020, 2020.

Sofieva, V. F., Rahpoe, N., Tamminen, J., Kyrölä, E., Kalakoski, N., Weber, M., Rozanov, A., von Savigny, C., Laeng, A., von Clarmann, T., Stiller, G., Lossow, S., Degenstein, D., Bourassa, A., Adams, C., Roth, C., Lloyd, N., Bernath, P., Hargreaves, R. J., Urban, J., Murtagh, D., Hauchecorne, A., Dalaudier, F., van Roozendaal, M., Kalb, N. and Zehner, C.: Harmonized dataset of ozone profiles from satellite limb and occultation measurements, *Earth Syst. Sci. Data*, 5(2), 349–363, doi:10.5194/essd-5-349-2013, 2013.

Sofieva, V. F., Tamminen, J., Kyrölä, E., Mielonen, T., Veefkind, P., Hassler, B. and Bodeker, G. E.: A novel tropopause-related climatology of ozone profiles, *Atmos. Chem. Phys.*, 14(1), 283–299, doi:10.5194/acp-14-283-2014, 2014.

Sofieva, V. F., Lee, H. S., Tamminen, J., Lerot, C., Romahn, F. and Loyola, D. G.: A method for random uncertainties validation and probing the natural variability with application to TROPOMI/Sentinel5P total ozone measurements, *Atmos. Meas. Tech. Discuss.*, 2020, 1–12, doi:10.5194/amt-2020-402, 2020.

Tatarskii, V. I.: *Wave Propagation in a Turbulent Medium*, edited by R. A. Silverman, McGraw-Hill, New York., 1961.

Veefkind, J. P., Aben, I., McMullan, K., Förster, H., de Vries, J., Otter, G., Claas, J., Eskes, H. J., de Haan, J. F., Kleipool, Q., van Weele, M., Hasekamp, O., Hoogeveen, R., Landgraf, J., Snel, R., Tol, P., Ingmann, P., Voors, R., Kruizinga, B., Vink, R., Visser, H. and Levelt, P. F.: TROPOMI on the ESA Sentinel-5 Precursor: A GMES mission for global observations of the atmospheric composition for climate, air quality and ozone layer applications, *Remote Sens. Environ.*, 120(0), 70–83, doi:<http://dx.doi.org/10.1016/j.rse.2011.09.027>, 2012.

Vira, J. and Sofiev, M.: On variational data assimilation for estimating the model initial conditions and emission fluxes for short-term forecasting of SO<sub>x</sub> concentrations, *Atmos. Environ.*, 46, 318–328, doi:<https://doi.org/10.1016/j.atmosenv.2011.09.066>, 2012.

Vira, J. and Sofiev, M.: Assimilation of surface NO<sub>2</sub> and O<sub>3</sub> observations into the SILAM chemistry transport model, *Geosci. Model Dev.*, 8(2), 191–203, doi:10.5194/gmd-8-191-

2015, 2015.

Vira, J., Carboni, E., Grainger, R. G. and Sofiev, M.: Variational assimilation of IASI SO<sub>2</sub> plume height and total column retrievals in the 2010 eruption of Eyjafjallajökull using the SILAM v5.3 chemistry transport model, *Geosci. Model Dev.*, 10(5), 1985–2008, doi:10.5194/gmd-10-1985-2017, 2017.

Wackernagel, H.: *Multivariate Geostatistics*, Springer., 2003.

Whitten, G. Z., Duel, H. P., Burton, C. S. and Haney, J. .: Overview of the implementation of an updated isoprene chemistry mechanism in CB4/UAM-V, *Memo. from Syst. Appl. Int.*, June, 1996.

WMO: *Meteorology — A three-dimensional science: Second session of the Commission for Aerology*, *WMO Bull.*, IV(4), 134–138, 1957.

Xian, P., Reid, J. S., Hyer, E. J., Sampson, C. R., Rubin, J. I., Ades, M., Asencio, N., Basart, S., Benedetti, A., Bhattacharjee, P. S., Brooks, M. E., Colarco, P. R., da Silva, A. M., Eck, T. F., Guth, J., Jorba, O., Kouznetsov, R., Kipling, Z., Sofiev, M., Perez Garcia-Pando, C., Pradhan, Y., Tanaka, T., Wang, J., Westphal, D. L., Yumimoto, K. and Zhang, J.: Current state of the global operational aerosol multi-model ensemble: An update from the International Cooperative for Aerosol Prediction (ICAP), *Q. J. R. Meteorol. Soc.*, 145(S1), 176–209, doi:<https://doi.org/10.1002/qj.3497>, 2019.

Yarwood, G. and Burton, S.: An Update to the Radical-Radical Termination Reactions in the CBM-IV, *Tech. Memo. Syst. Appl. Int.*, December [online] Available from: <http://airsite.unc.edu/soft/cb4/CB4docs.html>, 1993.

Ziemke, J. R., Chandra, S., Duncan, B. N., Froidevaux, L., Bhartia, P. K., Levelt, P. F. and Waters, J. W.: Tropospheric ozone determined from Aura OMI and MLS: Evaluation of measurements and comparison with the Global Modeling Initiative's Chemical Transport Model, *J. Geophys. Res. Atmos.*, 111(D19), n/a--n/a, doi:10.1029/2006JD007089, 2006.

Ziemke, J. R., Chandra, S., Labow, G. J., Bhartia, P. K., Froidevaux, L. and Witte, J. C.: A global climatology of tropospheric and stratospheric ozone derived from Aura OMI and MLS measurements, *Atmos. Chem. Phys.*, 11(17), 9237–9251, doi:10.5194/acp-11-9237-2011, 2011.